Available online at www.sciencedirect.com
ScienceDirect
Geochimica et Cosmochimica Acta 71 (2007) 3772–3795
Geochimica et Cosmochimica Acta
www.elsevier.com/locate/gca

Soils at the hyperarid margin: The isotopic composition of soil carbonate from the Atacama Desert, Northern Chile

Jay Quade [a,*], Jason A. Rech [b], Claudio Latorre [c,d], Julio L. Betancourt [e], Erin Gleeson [a], Mary T.K. Kalin [f]

[a] Department of Geosciences and the Desert Lab, University of Arizona, Tucson, AZ 85721, USA
[b] Department of Geology, Miami University, Oxford, OH 45056, USA
[c] CASEB-Departamento de Ecología, P. Universidad Católica de Chile, 114-D Santiago, Chile
[d] Institute of Ecology and Biodiversity (IEB), Universidad de Chile, Casilla 653, Santiago, Chile
[e] U.S. Geological Survey, 1675 West Anklam Road, Tucson, AZ 85745, USA
[f] Departamento de Ciencias Ecológicas, Universidad de Chile, Casilla 653, Santiago, Chile

Received 4 May 2006; accepted in revised form 12 February 2007; available online 2 March 2007

Abstract

We evaluate the impact of exceptionally sparse plant cover (0–20%) and rainfall (2–114 mm/yr) on the stable carbon and oxygen composition of soil carbonate along elevation transects in what is among the driest places on the planet, the Atacama Desert in northern Chile. $\delta^{13}C$ and $\delta^{18}O$ values of carbonates from the Atacama are the highest of any desert in the world. $\delta^{13}C$ (VPDB) values from soil carbonate range from −8.2‰ at the wettest sites to +7.9‰ at the driest. We measured plant composition and modeled respiration rates required to form these carbonate isotopic values using a modified version of the soil diffusion model of [Cerling (1984) *Earth Planet. Sci. Lett.* **71**, 229–240], in which we assumed an exponential form of the soil CO_2 production function, and relatively shallow (20–30 cm) average production depths. Overall, we find that respiration rates are the main predictor of the $\delta^{13}C$ value of soil carbonate in the Atacama, whereas the fraction C_3 to C_4 biomass at individual sites has a subordinate influence. The high average $\delta^{13}C$ value (+4.1‰) of carbonate from the driest study sites indicates it formed—perhaps abiotically—in the presence of pure atmospheric CO_2.

$\delta^{18}O$ (VPDB) values from soil carbonate range from −5.9‰ at the wettest sites to +7.3‰ at the driest and show much less regular variation with elevation change than $\delta^{13}C$ values. $\delta^{18}O$ values for soil carbonate predicted from local temperature and $\delta^{18}O$ values of rainfall values suggest that extreme (>80% in some cases) soil dewatering by evaporation occurs at most sites prior to carbonate formation. The effects of evaporation compromise the use of $\delta^{18}O$ values from ancient soil carbonate to reconstruct paleoelevation in such arid settings.

1. INTRODUCTION

The Atacama Desert is one of the driest places on earth, and as such presents an interesting opportunity to study the influence of plants on soil carbonate formation in an extreme setting. The possible connection between carbonate and life is of particular interest to those debating the significance of trace quantities of carbonate in Martian meteorites (McKay et al., 1996; Gibson et al., 2001) and dust (Banfield et al., 2003) as a possible indicator of life on Mars. In this paper we examine just one facet of life-carbonate relationship, the imprint of vascular plants on the carbon isotopic composition of soil carbonates. Most previous studies of the carbon isotopic composition of soil carbonate have focused on the relation to the local proportions of C_3, C_4 and CAM plants (e.g. Quade et al., 1995; Nordt et al.,

* Corresponding author. Fax: +1 520 792 8819.
E-mail address: quadej@email.arizona.edu (J. Quade).

0016-7037/$ - see front matter © 2007 Elsevier Ltd. All rights reserved.
doi:10.1016/j.gca.2007.02.016

1998; Fox and Koch, 2004; Zhisheng et al., 2005). While appropriate for moister areas, the additional variable of soil respiration rates and mixing with atmospheric CO_2 becomes important where plant cover is very sparse. In this paper we present our isotopic results from soil carbonate and organic matter in the Atacama Desert in northern Chile, the first systematic study from a hyperarid setting, but paralleling studies such as Amundson et al. (1988) and Quade et al. (1989) in the Mojave Desert. Previous modeling and analysis (Cerling, 1984; Quade et al., 1989) of modern soils have shown that the density and $\delta^{13}C$ value of plant cover are key determinants of the isotopic composition of soil carbonate. Our main objectives were to understand the relative contribution that these factors make to the isotopic composition of soil carbonate in the Atacama, and to determine whether all soil carbonate in such a sparsely vegetated region bears the isotopic imprint of biotic processes. To explore these and other relationships in the Atacama Desert, we surveyed plants and sampled soils along three transects (Figs. 1 and 2; Table 1). These include the Paposo transect (25°S; 0–2000 m), the Paso De Jama/Calama transect (22.5–23°S; 2500–4100 m), and the Socompa transect (24–24.5°S; 2900–4100 m). The Paposo Transect runs through the coastal fog-nourished "Lomas" zone into the western margin of the absolute desert. The other two transects extend at different latitudes from the eastern margin of the absolute desert into the upper elevation range of plants. The Socompa transect is located further south and is drier than the northern Paso de Jama transect. These plant survey results, combined with isotopic analysis of local vegetation, soil organic matter and recently formed soil carbonate, allow us to examine the influence of low soil respiration rates on the isotopic composition of soil carbonate. Comparison of these results with the isotopic composition of older soil carbonate allows us to examine possible long-term changes in plant cover.

The oxygen isotopic composition of carbonate in modern soils has received less systematic study than carbon isotopes in soil carbonate. Previous studies have shown that evaporation, in addition to temperature and the $\delta^{18}O$ value of rainfall, likely influence the $\delta^{18}O$ value of soil carbonates in deserts (Quade et al., 1989; Liu et al., 1996). Temperature and a few isotopic records of rainfall are available for the Atacama Desert, allowing us to estimate their contributions

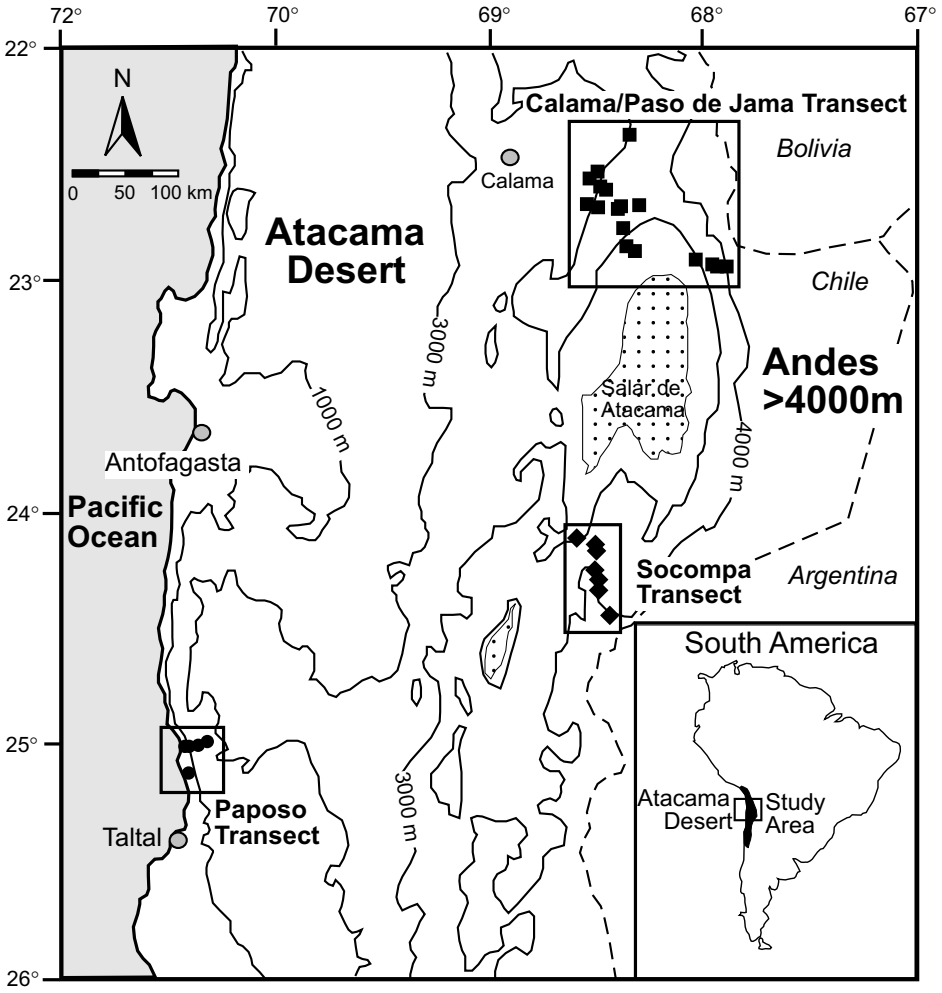

Fig. 1. General location of soil study areas in the central Atacama Desert. See Fig. 2 for details of insets.

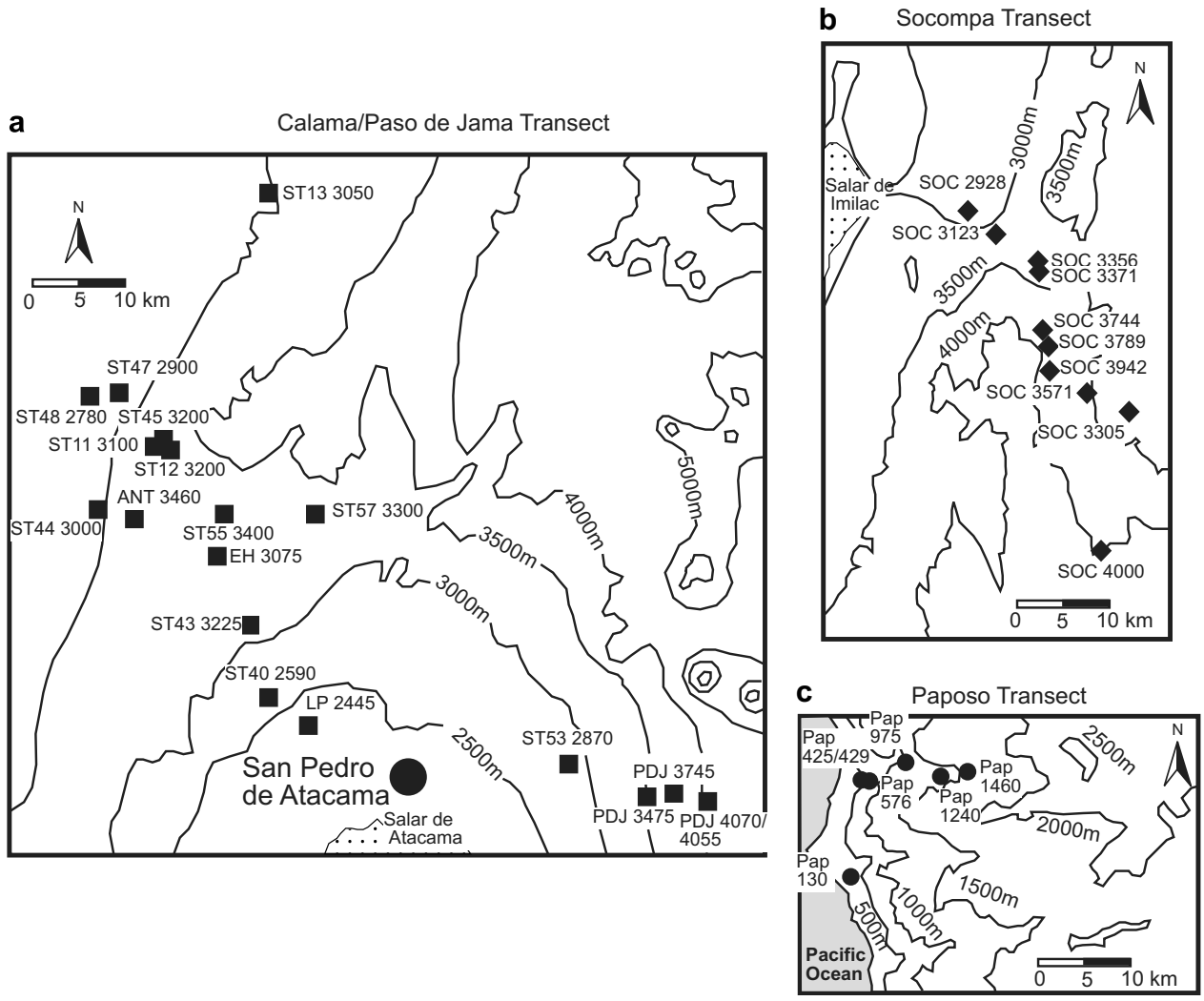

Fig. 2. Detailed location of soil sites along the three study transects: (a) Calama/Paso de Jama, (b) Socompa, and (c) Paposo.

to the $\delta^{18}O$ value of soil carbonates, as well as the role of evaporation, which should be all the more visible in a hyperarid setting like the Atacama.

1.1. Physiography and climate

The Atacama Desert occupies the narrow zone between the Andes and the Pacific Ocean (<300 km) from the Chilean/Peruvian border (18°S) south to about 27°S. It is bordered by a steep, ⩽2000 m-high escarpment that rises from the Pacific Ocean to the west, and by the high Andes (>5000 m) to the east. Moisture blockage by the Andes and the coastal escarpment, combined with a very cold Pacific Ocean, make the Atacama Desert among the driest regions on the planet (Trewartha, 1981; Houston and Hartley, 2003). The scant rain that does reach the region falls mostly on the coastal area (0–1500 m) and elevations above 2500–3000 m, whereas elevations between 1500 and 2500–3000 m are virtually rainless. Precipitation, which at higher elevations falls largely in the summer as convective storms fed by the South American Summer Monsoon system, lap over the high Andes and onto the upper Pacific slope (Garreaud, 1999; Vuille, 1999). Moisture nourishing the coastal areas is widely viewed as deriving largely from fog drip produced by the near-permanent coastal fogs or *camanchacas* (Rundel et al., 1991). Fog intensity is largely driven by a thermal inversion associated with large-scale subtropical subsidence. Water availability along the coast is also augmented by occasional Pacific storms (Cereceda et al., 2002).

Using compilations of meteorological stations from the region, we estimated mean annual rainfall and temperatures for all of our sample sites (Fig. 3; Table 1). Rainfall ranges from 114 mm/yr at the wettest site (4070 m), to virtually no rainfall in the absolute desert, to up to 12 mm/yr in coastal stations. Not represented in these coastal station totals is the contribution from fog drip, which at nearby Paposo showed a mean of 3.36 mm/day (1.2 m/yr) between 1999 and 2001 (Larrain et al., 2002) in trap nets at 750 m elevation. Mean annual temperature along our survey transects varies from ~18 °C along the coast to 2.6 °C at our highest elevation site at 4070 m.

Table 1
Transect site characteristics

Transect	Elevation	GPS coordinates datum: SA′56	MAT[a] (°C)	MAP[a] (mm/yr)	$\delta^{18}O$ (VSMOW)[b] rainfall	$\delta^{18}O$ (VSMOW)[c] Fog	Parent alluvial clasts
Paso de Jama	4070	19K 0616343, 7463902	2.6	114.1	−16.8		Ignimbrite
	3745	19K 0611766, 7465412	5.4	76.1	−13.9		Ignimbrite
	3475	19K 0608737, 7465796	7.5	56.3	−11.8		Ignimbrite
Socompa	4000	19J 0555502,7294288	3.2	104.4	−16.1		Basalt, andesite
	3942	19J 0550792, 7316053	3.7	97.0	−15.6		Granite, andesite, metasediments
	3789	19J 0550776, 7318816	5.0	80.2	−14.3		Granite, andesite, metasediments
	3744	19J 0550957,7314864	5.4	76.0	−13.9		Granite, volcanic
	3571	19J 0550776, 7318816	6.8	62.0	−12.5		Granite, volcanic
	3371	19J 0549100, 7326333	8.3	50.8	−11.1		Granite, volcanic
	3356	19J 0548378, 7326386	8.4	50.0	−11.0		Granite, volcanic
	3305	19J 0555903, 7314103	8.7	47.8	−10.6		Granite, volcanic
	3123	19J 0546019,7328963	10.0	41.0	−9.5		Granite, minor volcanic, metasediments
	2928	19J 0541597,7333562	11.2	35.4	−8.5		Granite, diorite, metasediments
Paposo	1460	19J 0365223, 7232703	17.2	0.0	−5.6	−1.9	Granite, volcanic
	1240	19J 0362032, 7231694	17.6	0.0	−5.6	−1.9	Granite, volcanic
	975	19J 0358895, 7233368	18.0	2.0	−5.6	−1.9	Granite, volcanic
	429	19J 0353912, 7232181	18.1	6.7	−5.6	−1.9	Granite, volcanic
	425	19J 0353729, 7231755	18.1	8.5	−5.6	−1.9	Granite, volcanic
	130	19J 0353912, 7232181	17.8	11.9	−5.6	−1.9	Volcanic

[a] Calculated from compilation from weather station data.
[b] Calculated using Eq. (7) in text, based on data from Fritz et al. (1981) and Aravena et al. (1999).
[c] From Aravena et al. (1989).

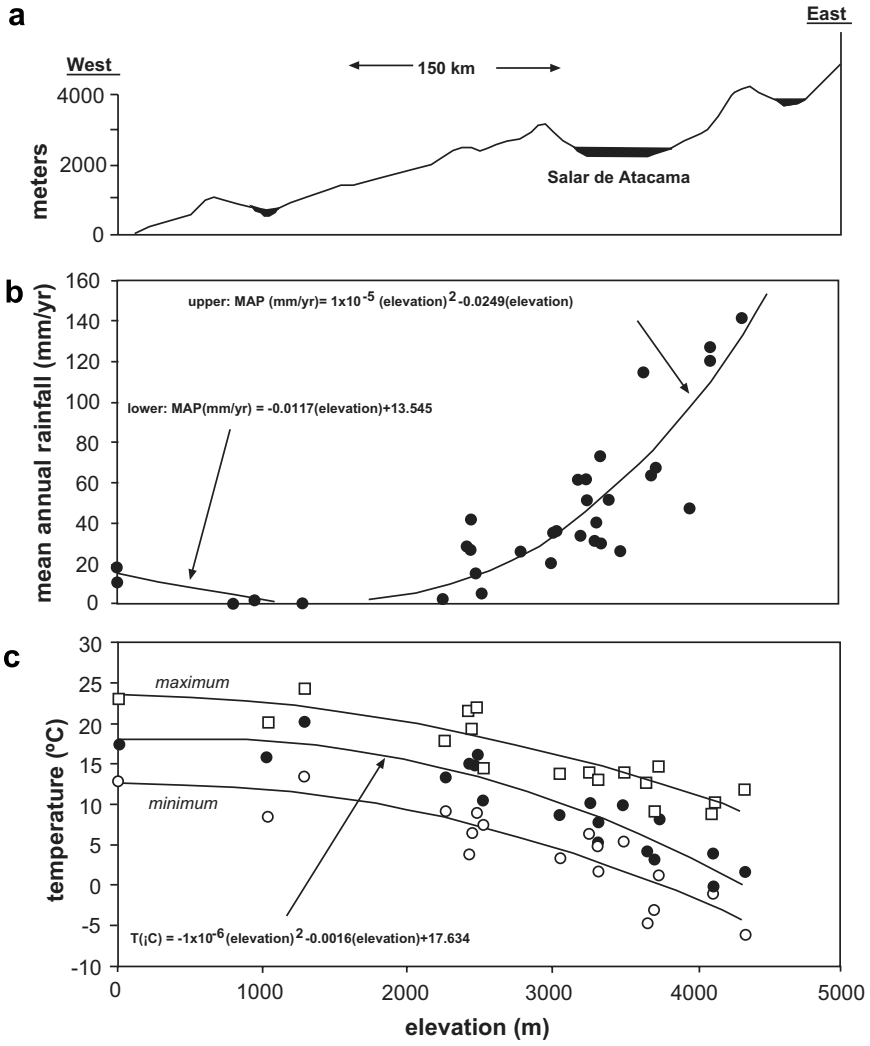

Fig. 3. (a) West–east topographic profile at ~23.5°S, (b) mean annual rainfall (mm/yr) (solid circles = weather station data), and (c) weather station data of monthly mean (solid circles), maximum (open squares), and minimum temperatures (open circles) (°C).

1.2. Vegetation and soil morphology

Floristically the Atacama Desert at 22–25°S can be divided into five major zones, reflecting the sharp climatic contrasts with elevation. The elevation limits of each zone vary locally according to slope aspect and drainage, and regionally due to higher rainfall at 22°S than at 24–25°S. The relatively narrow coastal zone (0–<1500 m) is dominated by fog-adapted Lomas "hill" vegetation (Rundel et al., 1991, 1996). The absolute desert extends inland about 100–150 km beyond Lomas, and is entirely plantless except along a few washes above 1500 m. We follow Villagrán et al. (1981, 1983) and Arroyo et al. (1988) for vegetation zones along the western slope of the Andes. The eastern margin of the absolute desert grades into the Pre-Puna (<30 mm/yr MAP), where shrubs and a few succulents compose the sparse vegetation cover. The shrubby Tolar zone (50–100 mm/yr MAP) extends from about 3200 to 4000 m. The high Andean steppe (100–200 mm/yr MAP), dominated by cold-tolerant C_3 grasses, extends from 4000 to 4500 m. Above ~4500 m, the Subnival is largely plantless. In the results section of this paper we present the detailed plant species composition at our study sites in each of these zones.

The morphology of sample soils varies considerably across the transects. In general we focused on gravelly soils on alluvial fans or on terraces in narrow canyons. Gravels in these deposits are dominated by granitic and some metasedimentary rocks along the coast, and volcanic rocks also with local metasediments on the Pacific slope of the Andes (Table 1). Carbonate clasts are rare to absent, thus insuring against detrital contamination of our secondary carbonate samples by local bedrock. No surface soil horizons (A horizons) in the transect show visible darkening from organic matter, except at few sites in the coastal Lomas zone. Lomas soils up to ~800 m do show moderate to strong reddening and clay enrichment (i.e. cambic or argillic horizons) in the upper 20–40 cm, underlain by variable accumulations of secondary carbonate. Dense cementation of gravels by carbonate is conspicuous on older terraces

paralleling canyons in the Lomas zone, but carbonate cementation drops off sharply by about 900–1000 m.

Anhydrite, halite, nitratite and many other salts dominate pedogenic mineralization in the absolute desert from about 1000–1500 m to 2500–3000 m (Ericksen, 1981; Searle and Rankin, 1993), often cementing soils to many meters depth. Secondary accumulations of clay, so visible in the coastal lomas soils, are not found. Only traces of carbonate are present in the soil matrix (Searle and Rankin, 1993; Berger and Cooke, 1997). We focused our sampling in this zone on very immature profiles with incipient salt accumulations.

Both reddish, clay-rich horizons, as well as abundant secondary carbonate, reappear in soils between about 3300 and 3800 m, coincident with increasing rainfall and the reappearance of plants. Above 4500 m, some soil reddening and secondary clay accumulation persists, although soil salts, including carbonate, do not.

We assigned relative stages of carbonate development (Stage I–IV) at each of our study sites, after the classification scheme of Gile et al. (1966). In this scheme, proceeding from young to old, Stage I refers to thin discontinuous coatings of carbonate on pebbles, Stage II to more continuous coats and some matrix cementation, Stage III to complete cementation of the matrix, and Stage IV to development of a dense laminar cap as downward percolation of soil water is inhibited by carbonate plugging of the matrix. Consistent with many previous studies, we assume that the Stage I to weak Stage II development of carbonate in our study soils required 10^3 to 10^4 years to develop, and Stages III–IV from 10^4 to 10^6 years (Machette, 1985). The focus of our sampling was on the very weakest carbonate development (Stage I–II) on young landforms close to active washes. Rodent midden evidence shows that vegetation has been largely stable over the last 3000 years and similar to today's, with minor changes in response to slightly increased rainfall in the mid and late Holocene (Betancourt et al., 2000; Latorre et al., 2002, 2005). We therefore make the assumption that incipient soil carbonate (Stage I–II) formed in the presence of plant cover similar to today's.

2. METHODS

2.1. Carbonate and organic matter

Pedogenic nodules and clast coatings were collected from freshly exposed trench faces or arroyo walls. All carbonate samples were heated at 250 °C for 3 h *in vacuo* and most processed using an automated sample preparation device (Kiel III) attached directly to a Finnigan MAT 252 mass spectrometer at the University of Arizona. In a few samples where % carbonate was low, CO_2 was extracted and purified off-line using 100% H_3PO_4 at 50 °C. $\delta^{18}O$ and $\delta^{13}C$ values were normalized to NBS-19 based on internal lab standards. Precision of repeated standards is $\pm 0.11‰$ for $\delta^{18}O$ and $\pm 0.07‰$ for $\delta^{13}C$ (1σ).

Soil organic matter was collected from 0 to 5 cm at 3–4 locations at a total of 16 transect sites (Tables 2a–2c). Samples were sieved through a 250 μm mesh sieve to remove coarse plant fragments, and amalgamated to yield a spatially averaged sample. Plant and bulk soil organic matter were pretreated with 2 M HCl and rinsed repeatedly with deionized water. Plant $\delta^{13}C$ values were measured using an automated CHN analyzer (Costech) connected to a Finnigan Delta-plus XL continuous-flow mass spectrometer. CO_2 from soil organic matter was extracted and purified off-line, and % organic C was determined manometrically. Internal lab standards are calibrated relative to NBS-22 and USGS-24. Precision of repeated internal standards is $\pm 0.09‰$ for $\delta^{13}C$ (1σ).

Carbonate and organic matter isotopic results are reported using standard δ-per mil notation relative to VPDB.

2.2. Plant survey methods

Most transect sites that we surveyed showed no signs of recent grazing or damage from herbivores, with the exception of PDJ-3745 (Table 1; Fig. 2a), where clear signs of grazing and trampling by domesticated llamas was evident. Thus we take the current condition of plant cover and composition at most sites as representative of late Holocene vegetation. Plant surveys were conducted in winter to early spring, and therefore failed to capture some of the summer annuals known to grow in the area.

The log-series survey method of McAuliffe (1991) was used to estimate plant cover and density for all perennial species at each soil site along the elevational transects. The McAuliffe method is a rapid survey technique appropriate for desert vegetation, where plant density is low (<25% total cover) and perennial ramets are distinct and separate. The size of the plot can be adjusted (in the Atacama we used from 8 to 250 m^2), depending on plant densities. In the Negev Desert, the McAuliffe method was found to provide more systematic relationships between environmental variables and vegetation gradients than other techniques such as Whittaker plots (Ward et al., 1993).

3. RESULTS

Isotopic results of this study consist of 63 analyses of vegetation, 19 analyses of soil organic matter, ~165 analyses of soil carbonate, and 32 analyses of fine-grained matrix carbonate in playas, soils, and dry washes. We first present our results of the composition, per cent cover, and $\delta^{13}C$ value of vegetation from our transects, along with the $\delta^{13}C$ value and concentration of soil organic matter, and then we give the isotopic results of soil carbonate (Figs. 5 and 6). We discuss the controls on the isotopic composition of soil carbonate in detail in the following section.

3.1. Plant density

Percent plant cover varies dramatically with elevation and to some extent with latitude in our study area (Fig. 4b; Table 2). In the Andes, the highest percentages of plant cover are attained in the Andean steppe dominated by the C_3 grasses *Stipa* and *Festuca* near Calama, and in the tolar by *Atriplex imbricata* and *Cistanthe salsoloides* along the Socompa transect. Predictably, per cent cover reaches higher values (19.4%) along the wetter Paso de Jama

Table 2a
Results of plant survey on the Paso de Jama transect

	Paso de Jama sites			$\delta^{13}C$ (‰)
	4070	3745	3475	
Plant taxa				
Stipa/Festuca	12.80	0.20		−24.59
Adesmia spinosissima	6.40			−22.50
Parastrephia lepidophylla	0.20			−20.66
Fabiana denudata		1.60		−21.51
Senecio aff. nutans		3.20		−22.77
Junellia seriphioides		0.20		−20.38
Chuquiraga atacamensis		0.03	0.20	−21.29
Atriplex imbricata		0.01	6.40	−14.14
Baccharis tola		0.03		−20.71
Opuntia sp.			0.20	−14.77
Lupinus			0.03	−22.76
Total % cover	19.4	5.3	6.8	
$\%C_4 + CAM$/total	0.0	0.2	96.7	
$\delta^{13}C$ from plot survey	−23.86	−22.33	−14.40	
Add 1.5‰	−22.36	−20.83	−12.90	
$\delta^{13}C$ of soil organic matter	−22.08	−20.61	−18.45	
Add 0.36‰	−21.72	−20.25	−18.09	
% Organic C	0.51	0.22	0.18	
Modeled respiration rate (mmole/m^2/h)	0.8	1.5	1.1	

transect than on the drier Socompa (14.4%) transect. Plant cover on both transects tapers to 0% between 4500 and 4700 m. The lower limit of the Andean vegetation (the Tolar zone) extends to 2900 m along the Calama transect, and to 3100 m along Socompa. The only major C_4 plant present in our surveys is *Atriplex imbricata*, which is significant (>40% of total plant cover) at about half the sites.

Plant density varies from <1% above about 1200 m to as high as 19.6% at 425 m along the Paposo transect in the Lomas zone (Fig. 4b; Table 2). Plant diversity and abundance is highly variable from year to year. Vegetation at the time of our survey was parched, with significant numbers of standing dead annuals. For comparison, Rundel and Mahu (1976) quantified plant cover along most of the same traverse up to 500 m. They measured some very high plant densities in the Lomas, up to 46%, particularly between 400 and 600 masl. Although some differences might be due to plot selection, size, and the method used, their measurements could also reflect conditions much closer to the growing season or a considerably wetter year.

3.2. Plant species

Our survey (Table 2c) reveals that the Lomas vegetation on our Paposo transect is densest and the most diverse along the coast below 600 m, where is it is dominated by the *Euphorbia lactiflua* (C_3), *Bahia ambosioides* (C_3), succulents such as *Copiapa cinera* (CAM) and *Eulychnia iquiquensis* (CAM), several species of *Nolana*, and herbaceaous *Cristeria intergerrima*. As vegetation thins above 1000 m, *Huidobria fruticosa* and *Nolana leptophylla* dominate the few plants present. Plants in the Lomas are all C_3 except a few CAM plants and C_4 plants, including *Atriplex mucronata*, *Cistanthes* sp., and one species of *Nolana* (Table 2c), none of which ever dominate over C_3 plants at any site.

The eastern margin of the absolute desert is defined by the lower limit of the Pre-Puna zone; common plants include *Cistanthe salsoloides* (C_3), *Gilia crassifolia* (C_3), *Acantholippia deserticola* (C_3), *Ephedra breana* (C_3), and the halophyte *Atriplex imbricata* (C_4). The Tolar zone (or Puna belt, e.g. Ruthsatz, 1977) (50–100 mm/yr MAP) extends from about 3200 to 4000 m. *Fabiana denudata* (C_3), in association with *Baccharis tola* and *B. boliviensis* (C_3), dominate the lower part of the tolar, and *Parastrephia quadrangularis* (C_3), and *P. lepidophylla* (C_3), dominate between 3700 and 4000 m. In contrast to the perennial shrubs which are nearly all C_3, the annual summer grasses in the tolar are commonly C_4, including *Aristida adscensionis*, *Bouteloua simplex*, *Enneapogon devauxii*, and *Munroa decumbens*.

The high Andean steppe zone (100–200 mm/yr MAP) extends from 4000 to 4500 m. A variety of grasses, dominated by *Festuca chrysophylla* (C_3) to the north and by *Deyeuxia* spp., and *Stipa frigida* (C_3), to the south, characterize much of steppe zone. The Subnival (or high alpine zone, >4500 m) above the Andean steppe is almost plantless except for sparse perennials and a few cushion plants such as *Azorella* and *Pycnophyllum*.

Carbon isotopic results from plants confirm what our field survey suggested, that most of the plants along the transect are C_3's. The average of all C_3 plants along the transect is −23.1‰. This average is markedly higher than global average values of around −27‰ for C_3 plants, and is consistent with the higher water-use efficiency displayed by desert C_3 plants (e.g. Ehleringer, 1988). Although C_4 and CAM plants are present at about half of the sample sites, they only dominate the overall flora at four sites (Fig. 2a; Table 2). These include *Atriplex mucronata* ($\delta^{13}C(VPDB) = -15.7‰$), *Atriplex imbricata* (−15.0‰ and −14.1‰) among the shrubs, and *Cistanthe pachyphylla*

Table 2b
Results of plant survey on the Socompa Transect

	Socompa site numbers								$\delta^{13}C$ (‰)
	4000	3942	3789	3744	3571	3356	3305 Pampa de Inca	3123	
Plant taxa									
Stipa frigida	3.20		0.03				0.00		−22.8
Adesmia melanthes	1.60		1.60	0.10	0.03				−21.8
Jaborosa parviflora	1.60								−22.5
Doniophyton cf. weddellii	0.03								−27.9
Cristaria andicola	0.05		0.05	0.80	0.40				−24.2
Phacelia cummingii	0.00								−23.3
Atriplex imbricata		6.40	6.40	0.80	1.60	1.60	6.40	0.10	−15.2
Reyesia parviflora			0.80						−21.6
Ephedra sp.			1.60						−22.1
Unknown *Solanacae*			0.00						
Gilia crassifolia				0.20		0.10	0.10		−23.3
Opuntia					0.40		0.10		
Artemisia copa					0.20				−21.6
Haplopappus rigidus					0.01				−21.7
Cryptantha					0.20				
Adesmia erinacea					0.20				
Cistanthe salsoloides						12.80		3.20	−22.9
Cistanthe amaranthoides								3.20	−21.3
Total % cover	6.5	6.4	10.5	1.9	3.8	14.5	6.6	6.5	
$\%C_4 + CAM$/total	0.0	100.0	61.1	42.1	52.6	11.0	97.0	1.5	
$\delta^{13}C$ from plot survey	−22.54	−15.22	−17.82	−20.21	−17.00	−22.02	−15.11	−21.97	
Add 1.5‰	−21.04	−13.72	−16.32	−18.71	−15.50	−20.52	−13.61	−20.47	
$\delta^{13}C$ of soil organic matter	−23.68		−23.79	−20.82	−20.24	−22.57	−21.38	−26.01	
Add 0.36‰	−23.32		−23.43	−20.46	−19.88	−22.21	−21.02	−25.65	
% Organic carbon	0.22		0.20	0.44	1.20	0.13	0.13	0.06	
Modeled respiration rate (mmole/m^2/h)	0.1		0.1	0.3		0.2	0.2	0.0	

Table 2c
Results of plant survey on the paposo transect

	Paposo site numbers						$\delta^{13}C$ (‰)
	1460	1240	975	429	425	130	
Plant Taxa							
Huidobria fruticosa	1.60	1.60					−22.4
Cistanthe sp.	0.05	0.20					−18.4
Nolana leptophylla		0.80					−21.7
Nolana villosa			0.40				−22.3
Nolana linearifolia			0.80				−21.2
Tetragonia macrocarpa			0.40				−21.9
Gypothamnium pinnifolium			0.80				−22.3
Echinopsis deserti				0.80	3.20		−23.5
Cristaria cf. maritima				0.40	1.60	3.20	−22.3
Bahia ambrisoides				6.40			−25.3
Euphorbia lactiflua				1.60		12.80	−22.6
Solanum sp.				0.10			ND
Proustia cuneifolia				1.60			−25.1
SOC 429 unknown 2				0.10			−24.1
Copiapoa				0.01		0.20	−8.9
Eulychnia iquiquensis				3.20		1.60	−15.0
Chenopodium aff. pinnatum				0.05			−24.3
Solanum (big leaf)				0.05			ND
Atriplex mucronata				0.80			−15.1
Nolana ramosissima				0.40			−23.1
Brassiacoae				0.01			−25.6
Polychryus				0.00			−20.7
Lycium				1.60			−27.2
Nolana peruviana					12.80		−23.8
Frankenia chilensis					1.60		−22.1
Mesembryanthemum crystallinum					0.40		−13.9
Total % cover	1.65	2.60	2.40	17.12	19.60	17.80	
$\%C_4$ + CAM/total	0	0	0	23.40	2.04	0	
$\delta^{13}C$ from plot survey	−22.24	−21.85	−21.87	−22.37	−23.34	−21.73	
Add 1.5‰	−20.74	−20.35	−20.37	−20.87	−21.84	−20.23	
$\delta^{13}C$ of soil organic matter	−26.35	−24.35	−26.5	−22.13	−24.12	−21.5	
Add 0.36‰	−25.99	−23.99	−26.14	−21.77	−23.76	−21.14	
% Organic C	0.06	0.05	0.07	12.7	2.85	1.63	
Modeled respiration rate (mmole/m^2/h)	0	0	1	3.7	2	1.8	

(−16.4‰). CAM plants are sparse and include *Opuntia* sp. (−11.2‰) on the Paso de Jama transect and several CAM species in the lomas.

The bulk $\delta^{13}C$ composition of plants ($\delta^{13}C_{bulk}$) can be estimated from the isotopic composition of each plant weighted by the fraction cover for that plant (Table 2). This estimate provides useful insights into the origin of the $\delta^{13}C$ value of soil-respired CO_2 ($\delta^{13}C_{resp}$) discussed later in the paper.

3.3. Soil organic matter

Percent organic carbon is highly variable in most Atacama soils, and ranges from <0.03% in the absolute desert (Drees et al., 2006), 0.05–0.06 at near-plantless sites on the fringes of the absolute desert, to much higher values of 5–12% in the middle of the coastal Lomas zone (Fig. 4c; Table 2). $\delta^{13}C$(VPDB) values of soil organic matter ($\delta^{13}C_{som}$) at transect sites vary between −18.1 and −26.1‰ (Fig. 4d; Table 2). The highest values come from sites such as PDJ-3475 and SOC 3744 where *Atriplex imbricata*, a C_4 plant, is abundant. Quite interestingly, the lowest values come from the near-plantless sites on the fringes of the absolute desert.

3.4. Soil carbonate

3.4.1. Carbon isotopes

$\delta^{13}C$ values of soil carbonate ($\delta^{13}C_{sc}$) of all ages show a very broad range in the Atacama, from −8.2‰ to +7.9‰ (Fig. 5; Table 3). Very high (>+2‰)$\delta^{13}C_{sc}$ values tend to be found (1) at shallow (<20 cm) depths in most soils, (2) in sites bordering the absolute desert along the Paposo (Table 3: Paposo 1240 and 1460) and Calama (Table 3: Llano de la Paciencia 2445) transects, (3) in all sites and at all soil depths within the hyperarid absolute desert (Table 3: AT-987, −1240, −1315, −1921, −2510, 2792), and (4) in many sites along the very dry Socompa Transect. The most negative $\delta^{13}C$ values (<−5‰) are associated with coastal Lomas zone, and mid-elevation sites (Table 3: AT sites between 3120 and 3300 m) along the Calama transect. In the coastal Lomas zone, $\delta^{13}C_{sc}$ values increase with elevation

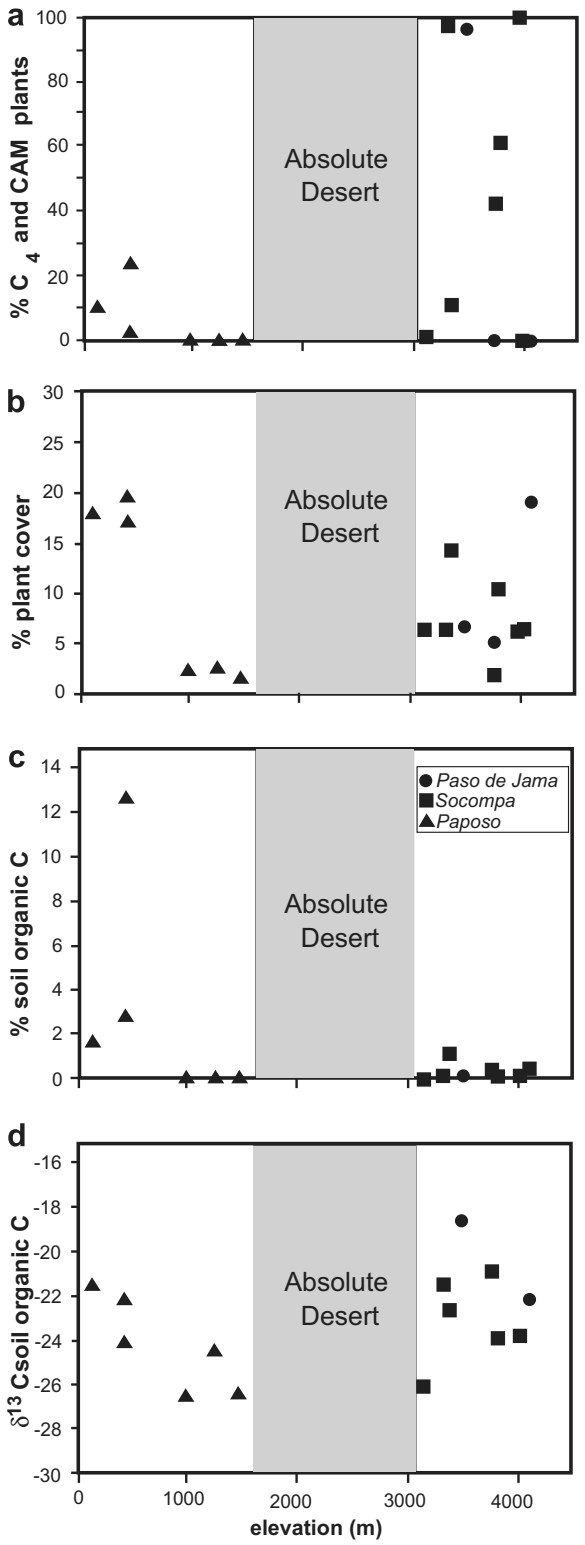

Fig. 4. (a) % C_4 + CAM plants, (b) % plant cover, (c) % soil organic matter, and (d) $\delta^{13}C$ (VPDB) of soil organic matter, all versus elevation (m).

(0–1460 m). Soil carbonate picks up again at 2500–3000 m, and $\delta^{13}C_{sc}$ values decrease with elevation increase to ~4000 m (Fig. 5).

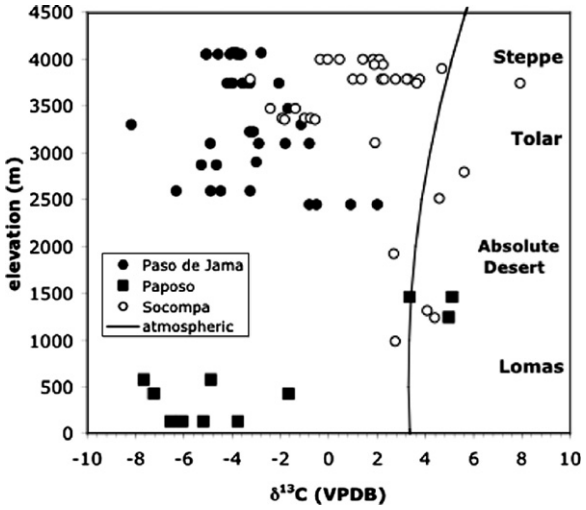

Fig. 5. $\delta^{13}C$ (VPDB) of soil carbonate versus elevation for >50 cm soil depths, all Stage I–II development only. Also plotted is the modeled $\delta^{13}C$ value of carbonate formed in isotopic equilibrium with pre-industrial atmospheric CO_2. The precise elevation boundaries between vegetation zones are not indicated since they vary in the study area with latitude.

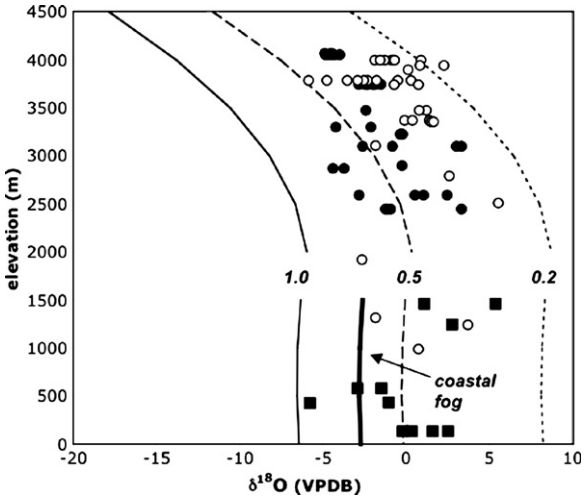

Fig. 6. $\delta^{18}O$ (VPDB) value of soil carbonate versus elevation for >50 cm soil depths, all Stage I–II development only (see Fig. 5 for symbol legend). Also shown are lines depicting the fraction of moisture remaining after evaporation ($f = 1.0$ or 0% evaporation; $f = 0.2$ or 80% evaporation) at 100% humidity from the soil, assuming local rainfall reported in Aravena et al. (1999) and Fritz et al. (1981) as the moisture source. For the low (<1000 m) elevations, starting values for both local rainfall and fog at $f = 1$ (no evaporative loss) shown.

$\delta^{13}C$ values of carbonate in silt-rich samples from phreatic and dry playas, the upper ~5 cm of several soils, and silt peels in dry washes in or on the margin of the absolute desert are higher (Table 4; mean = +1.3 ± 2.9‰, $n = 26$) than average soil carbonate values (mean = −1.4 ± 3.4‰).

Table 3
Stable isotopic analyses from Atacama soil carbonates

Sample ID	Elevation (m)	Depth (cm)	Form	Stage	$\delta^{13}C$ PDB	$\delta^{18}O$ PDB
Calama transect						
Paso de Jama 4070 m (19K 0616343 7463902)						
PDJ 4070 −107	4070	−107	Coating	I	−2.80	−4.50
PDJ 4070 −127	4070	−127	Coating	I	−4.00	−4.89
PDJ 4070 −133	4070	−133	Coating	I	−3.80	−4.50
PDJ 4070 −147	4070	−147	Coating	I	−3.90	−4.50
PDJ 4055 m (19K 0615175 7464855)						
PDJ 4055 A/115A	4055	−115	Fracture	I	−4.58	−4.60
PDJ 4055a/115B	4055	−115	Fracture	I	−5.07	−4.81
PDJ 4055A/115C	4055	−115	Fracture	I	−5.07	−4.83
PDJ 4055B/115A	4055	−115	Fracture	I	−3.62	−4.32
PDJ 4055B/115B	4055	−115	Fracture	I	−3.69	−3.98
PDJ 4055B/115C	4055	−115	Fracture	I	−3.82	−4.41
PDJ 4055B/115D	4055	−115	Fracture	I	−4.09	−4.40
Paso de Jama 3745 m (19K 0611766 7465412)						
PDJ 3745 −52 (sect.1)	3745	−52	Coating	I	−3.57	−2.00
PDJ 3745 −66	3745	−66	Coating	I	−4.20	−2.32
PDJ 3745 −95 (pebble 2)	3745	−95	Coating	I	−3.54	−2.47
PDJ 3745 −95	3745	−95	Coating	I	−3.98	−2.85
PDJ 3745 −120	3745	−120	Coating	I	−3.29	−2.34
PDJ 3745 −160	3745	−160	Coating	I	−3.28	−1.95
PDJ 3745 −160 (pebble 2)	3745	−159	Coating	I	−4.07	−1.52
PDJ 3745 −175	3745	−175	Coating		−2.06	−1.86
Paso de Jama 3475 m (19K 0608737 7465796)						
PDJ 3475 −35	3475	−35	Coating	I	−5.20	−1.23
PDJ 3475 −74	3475	−74	Coating	I	−1.70	−2.42
PDJ 3475 −120	3475	−120	Coating		−1.27	−0.93
Antenna 3460 m (19K 0561453 7489448)						
ANT 3460 −13	3460	−13	Coating	I	4.50	−1.53
ANT 3460 −24	3460	−24	Coating	I	1.60	−2.42
ANT 3460 −51	3460	−51	Coating	I	1.50	−4.30
AT16 3465 −62	3465	−62	Coating	I	−0.70	−5.89
AT17 3465 −120	3465	−120	Coating	I	−1.90	−4.40
AT18 3465 −85	3465	−85	Coating	III	2.20	−1.03
AT19 3465 −140	3465	−140	Coating	III	−3.00	−1.43
St. 55 3400 m (19K 0562156 7493351)						
AT402 3400 −20	3400	−20	Coating	II	−1.74	1.46
AT403 3400 −35	3400	−35	Coating	II	−0.50	−3.27
AT409 3400 −33	3400	−33	Coating	I	0.18	0.51
AT410 3400 −41	3400	−41	Coating	I	1.00	1.04
St. 57 3300 m (19K 0572527 7492795)						
AT416 3300 −50	3300	−50	Coating	I	−8.17	−4.23
AT412 3300 −220	3300	220	Coating	I	−1.15	−2.12
St. 43 3225 m (19K 0564194 7481812)						
AT330 3225 −25	3225	−25	Coating	II	−1.89	0.40
AT331 3225 −60	3225	−60	Coating	II	−3.28	−0.34
AT332 3225 −85	3225	−85	Coating	II	−3.11	−0.23
St. 12 3200 m (19K 0556682 7501690)						
AT89 3200 −55	3200	−55	Coating	I	−7.20	−2.91
AT90 3200 −120	3200	−120	Coating	II	−1.20	−1.23
AT93 3200 −150	3200	−150	K horizon	III	−4.90	−4.30
AT92 3200 −225	3200	−225	Coating	II	−4.70	−4.70
AT91 3200 −275	3200	−275	Coating	II	−4.30	−4.70
AT95 3200 −25	3200	−25	K horizon	IV	−5.30	−4.20
AT96 3200 −45	3200	−45	K horizon	IV	−5.00	−5.49
AT97 3200 −95	3200	−95	K horizon	IV	−4.80	−4.50

Table 3 (*continued*)

Sample ID	Elevation (m)	Depth (cm)	Form	Stage	$\delta^{13}C$ PDB	$\delta^{18}O$ PDB
St. 45 3200 m (19K 0556925 7503551)						
AT342 3205	3205	exposed	K horizon	III	−4.69	−3.84
AT343 3205	3205	exposed	K horizon	III	−2.17	−3.61
AT344 3210	3210	exposed	K horizon	III	−4.43	−2.23
AT345 3185	3185	exposed	K horizon	IV	−6.03	−3.61
AT346 3185	3185	exposed	K horizon	IV	−4.33	−3.11
AT34B 3180	3180	exposed	K horizon	III	−3.54	−3.89
AT348 3180	3180	exposed	K horizon	IV	−2.75	−1.13
St. 11 3100 m (19K 0554530 7503230)						
AT84 3100 −15	3100	−15	Coating	I	−2.50	0.55
AT85 3100 −55	3100	−55	Coating	I	−0.80	3.33
AT86 3100 −75	3100	−75	Coating	I	−2.90	3.03
AT87 3100 −100	3100	−100	Coating	II	−4.90	−0.83
AT88 3100 −135	3100	−135	Coating	I	−1.80	−2.62
El Hotel 3075 m (19K 0552670 7492384)						
EH 3075 −2	3075	−2	Coating	I	−1.60	−3.21
EH 3075 −40	3075	−40	Matrix		−2.40	0.36
EH 3075 −40	3075	−40	Coating	I	−0.70	−3.51
EH 3075 −64	3075	−64	Coating	I	−0.50	−5.59
EH 3075 −90	3075	−90	Coating	I	−1.00	−4.89
AT15 3120 −82	3120	−82	K horizon	II	−5.10	−1.23
AT13 3120 −95	3120	−95	K horizon	III	−4.50	−1.82
AT14 3120 −105	3120	−105	K horizon	III	−4.60	−2.42
St. 13 3050 m (19K 0567631 7528323)						
13B 3050 +280	3050	−20	K horizon	III	−1.49	2.35
13B 3050 +260	3050	−35	K horizon	IV	−0.99	0.79
13B 3050 +235	3050	−60	K horizon	IV	−2.44	−0.15
13B 3050 +215	3050	−85	K horizon	IV	−2.09	0.06
13B 3050 +200	3050	−100	K horizon	IV	−2.53	−2.09
13B 3050 +150	3050	−150	K horizon	IV	−3.43	−2.09
13B 3050 +115	3050	−190	K horizon	III	−2.98	−2.60
13B 3050 +80	3050	−215	Coating	I	−1.18	0.23
St. 44 3000 m (19K 0548670 7494410)						
AT341 3000	3000	exposed	K horizon	III	−2.61	−1.20
St. 47 2900 m (19K 0551533 7505841)						
AT352 2900 −25	2900	−25	Coating	II	−3.58	−0.27
AT351 2900 −70	2900	−70	Coating	II	−3.00	−0.25
St. 53 2870 m (19K 0600086 7465750)						
AT393 2870m −54	2870	−54	Vein	I	−4.65	−3.73
AT394 2870m −75	2870	−75	Vein	I	−5.27	−4.40
St. 48 2780 m (19K 0547053 7506303)						
AT352B 2780 −70	2780	−70	Coating	II	−1.31	2.99
AT353 2780 −120	2780	−120	K horizon	III	−1.48	2.88
St. 40 2590 m (19K 0567867 7472840)						
AT322 2590 −10	2590	−10	Coating	I	−2.36	0.55
AT321 2590 −75	2590	−75	Coating	I	−3.26	2.46
AT320 2590 −115	2590	−115	Coating	I	−4.47	1.05
AT319 2590 −160	2590	−160	Coating	I	−4.89	0.53
AT318 2590 −210	2590	−210	Coating	I	−6.31	−2.83
Llano de la Pacienca 2445 m (19K 0571092 7470197)						
LP 2445 −10	2445	10	Matrix	I	−1.40	−4.40
LP 2445 −10	2445	−10	Coating	I	4.40	1.05
LP 2445 −30	2445	−30	Coating	I	5.80	0.36
LP 2445 −50	2445	−50	Coating	I	2.00	3.33
LP 2445 −70	2445	−70	Coating	I	0.90	−0.93
LP 2445 −90	2445	−90	Coating	I	−0.80	−1.13
LP 2445 −190	2445	−190	Coating	I	−0.50	−1.23

(*continued on next page*)

Table 3 (*continued*)

Sample ID	Elevation (m)	Depth (cm)	Form	Stage	$\delta^{13}C$ PDB	$\delta^{18}O$ PDB
Quebrada Paposo transect						
Paposo 1460 m (19J0365223 7232703)						
POP 1460 −20	1460	−20	silt in void	I	3.71	1.65
POP 1460 −20	1460	−20	Coating	I	4.02	−1.00
POP 1460 −60	1460	−60	Coating	I	5.11	5.40
POP 1460 −70	1460	−70	Coating	I	3.34	1.11
Paposo 1240 m (19J0362085 7231734)						
POP 1245 −35	1245	−35	Matrix		4.38	3.71
POP 1245 −100	1245	−100	Coating	I	4.98	2.76
Paposo 576 m (19J 0355010 7232610)						
POP 576 −5	576	−5	Matrix	I	−4.02	−8.42
POP 576 −20	576	−20	Coating	I	−6.11	−0.47
POP 576 −75	576	−75	Coating	I	−7.65	−1.48
Paposo 429 m (19J 0353912 7232181)						
POP 425 −20	429	−20	Coating	I	−3.65	−0.19
POP 425 −35	429	−35	Coating	I	−7.09	−2.40
POP 425 −70	429	−70	Coating	I	−7.23	−1.03
Paposo 425 m (19J 0353729 7231755)						
POP 425 −100	425	−100	K horizon	III	−7.01	−1.96
POP 425 −300	425	−300	K horizon	III	−6.88	−1.11
POP 425 −325	425	−325	K horizon	III	−6.80	−0.76
Paposo 130 m (19J 0351763 7222492)						
POP 130 0-2av	130	−1		II	−5.54	0.97
POP 130 −35	130	−35	Coating	II	−4.19	1.91
POP 130 −50	130	−50	Coating	II	−5.18	1.60
POP 130 −70	130	−70	Coating	I	−6.06	0.36
POP 130 −100	130	−100	Coating	I	−6.54	−0.21
POP 130 −120		−120	Coating		−3.76	2.54
Blanco Encalado (19J 0356341, 7316528)						
Blanco Encalado 1750	1750		Coating	III	−2.41	0.51
Socompa transect						
Socompa 4000 m (19J 0555502 7294288)						
SOC 4000 #3	4000	−37	Matrix	I	0.00	0.98
SOC 4000 #2	4000	−52	Matrix	I	−0.35	0.89
SOC 4000 #1	4000	−70	Coating	I	1.84	−0.87
SOC 4000C	4000	>−50	Coating	I	−0.05	−1.29
SOC 4000D	4000	>−50	Coating	I	1.41	−0.69
SOC 4000A	4000	>−50	Coating	I	2.10	−1.88
SOC 4000E	4000	>−50	Coating	I	0.44	−1.55
Socompa 3942 m (19J 0550792 7316053)						
SOC 3942 #6	3942	−3	Matrix?	I	2.34	4.35
SOC 3942 #5	3942	−25	Matrix?	I	2.99	4.35
SOC 3942 #4	3942	−35	Matrix?	I	3.71	6.39
SOC 3942 #3	3942	−45	Matrix?	I		
SOC 3942 #2	3942	−52	Matrix?	I	2.24	2.28
SOC 3942 #1	3942	−70	Matrix?	I	1.88	0.83
Socompa 3789 m (19J 0550772 7318816)						
SOC 3788 −44	3788	−44	Coating	I	4.32	0.51
SOC 3788 −55	3788	−55	Coating	I	2.18	−5.85
SOC 3788 −80	3788	−80	Coating	I	−3.26	−4.76
Socompa 3789 m (19J 0550772 7318816)						
SOC 3788/60/70A/19	3788	−60	Coating	I	1.00	−2.30
SOC3788/60/70B	3788	−60	Coating	I	1.36	−2.56
SOC 3788/60/70C	3788	−60	Coating	I	2.29	−0.50
SOC 3788 UN B	3788	ND	Coating	I	3.29	−2.91
SOC 3788 UN C	3788	ND	Coating	I	2.77	−1.77
SOC 3789 35/50B	3788	−42.5	Coating	I	3.75	−3.54

Table 3 (*continued*)

Sample ID	Elevation (m)	Depth (cm)	Form	Stage	δ^{13}C PDB	δ^{18}O PDB
SOC 3789 35/50C	3788	−42.5	Coating	I	3.23	0.30
Socompa 3744 m (19J 0550264 7319675)						
SOC 3743 0-1 Av	3743	−1	Matrix	I	0.64	−1.49
SOC 3743 −8	3743	−8	Coating	I	3.72	−0.09
SOC 3743 −25	3743	−25	Coating	I	5.63	−0.14
SOC 3743 −45	3743	−45	Coating	I	7.93	−0.72
SOC 3743 −63	3743	−63	Coating	I	3.63	0.75
Socompa 3475 m						
SOC 3475/100A	3475	−100			−2.42	1.22
SOC 3475 /100B	3475	−100			−1.38	0.79
Socompa 3371 m (19J 0549100 7326333)						
SOC 3371 #1	3371	−12	Matrix?	I	5.35	5.65
SOC 3371 #2	3371	−82	Coating?	II	−1.01	1.39
SOC 3371 #3	3371	−105	Coating	II	−0.76	−0.09
SOC 3371 #4	3371	−130	Coating	II	−1.93	0.37
Socompa 3356 m (19J 0541597 7333562)						
SOC 3356 −7	3356	−7	Coating	I	5.27	3.72
SOC 3356 −38	3356	−38	Coating	I	3.34	6.51
SOC 3356 −55	3356	−55	Coating	I	−1.82	1.49
SOC 3356 −70	3356	−70	Coating	I	−0.56	1.65
Socompa 3123 m (19J 0546019 7328963)						
SOC 3123/5/15A	3123	7.5	Coating	I	6.35	0.34
SOC 3123/5/15B	3123	7.5	Coating	I	7.42	0.77
Socompa 2928 m (19J 0541597 7333562)						
SOC 2928- 10	2928	−10	Coating	I	3.07	7.29
Socompa 3305 m (Pampa de Inca) (19J 0555903, 7314103)						
AD04-46I/165/170A	3305	−165	K horizon	IV	−2.42	−1.98
AD04-46I/165/170C	3305	−165	K horizon	IV	−2.16	−1.82
AD04-46I/100/105A	3305	−100	K horizon	IV	−0.36	−2.12
AD04-46I/100/105B	3305	−100	K horizon	IV	−0.87	−1.89
AD04-46I/100/105C	3305	−100	K horizon	IV	−0.85	−2.38
AD04-46 I/70/80B	3305	−70	K horizon	IV	−1.02	−1.22
AD04-46 I/70/80C	3305	−70	K horizon	IV	−0.18	0.99
AD04-46II/65A	3305	−65	K horizon	IV	−1.14	0.26
AD04-46II/65B	3305	−65	K horizon	IV	−0.31	1.03
AD04-46II/65C	3305	−65	K horizon	IV	2.05	2.14
AD04-46II /100/110A	3305	−100	K horizon	IV	3.23	2.76
AD04-46III/110/120A	3305	−110	K horizon	IV	−0.99	−1.15
AD04-46III/110/120B	3305	−110	K horizon	IV	−0.85	−1.05
AD04-46III/110/120C	3305	−110	K horizon	IV	−0.69	−0.82
AD04-46 III/85/90A	3305	−85	K horizon	IV	−0.93	−1.94
AD04-46 III/85/90B	3305	−85	K horizon	IV	0.39	0.38
AD04-46 III/85/90C	3305	−85	K horizon	IV	−0.77	−1.40
AD04-46 IIII/150A	3305	−150	K horizon	IV	−1.55	−1.19
AD04-046 IIII/150B	3305	−150	K horizon	IV	−2.99	−3.17
AD04-46 IIII/150C	3305	−150	K horizon	IV	−1.34	−0.48
19Q 0361578, 2627150						
AT425	425	30–40 cm	Matrix		−1.78	−6.27
19R 0377825, 2662582						
AT987	987	30–40 cm	Matrix		2.76	0.74
19R 0453395, 2694514						
AT1315	1315	30–40 cm	Matrix		4.07	−1.84
19R 0458807, 2753534						
AT1921	1921	30–40 cm	Matrix		2.69	−2.65

(*continued on next page*)

Table 3 (*continued*)

Sample ID	Elevation (m)	Depth (cm)	Form	Stage	$\delta^{13}C$ PDB	$\delta^{18}O$ PDB
19R 0476153, 2691817						
AT2510	2510	30–40 cm	Matrix		4.58	5.54
19R 0480631, 27243122						
AT2792	2792	30–40 cm	Matrix		5.60	2.60
19R 0517177, 27039403						
AT3107	3107	30–40 cm	Matrix		1.91	−1.84

Table 4
Isotopic results from non-soil carbonates

Sample no.	Elevation (masl)	Latitude (S)	Longitude (W)	$\delta^{13}C$ VPDB	$\delta^{18}O$ VPDB	% $CaCO_3$	Comments
AD04-3	1248	24°6.356′	70°13.748′	2.95	6.52	2.6	Near Soc 987, silt under rock
AD04-6	1122	24°01.723′	69°39.476′	2.83	−2.18	1.4	Silt peel in floodway, Quebrada Chimborzo
AD04-8	1525	23°24.101′	69°27.531′	2.95	−1.09	1.8	Wash silt
AD04-10	2464	23°32.582′	68°50.295′	5.05	2.16	0.8	Unamed playa east pf Elvira
AD04-13	2917	23°40.244′	68°40.099′	4.23	7.03	1.5	Silt from Av, between Salar de Atacam and Elvira
AD04-14	2347	23°39.697′	68°34.358′	−1.37	−3.35	5.4	SW corner of Salar de Atacama
AD04-15	2372	23°39.479′	68°32.358′	−4.23	−5.76	2.8	Silt, Salar de Atacama, SW
AD04-19	2392	23°08.672′	68°02.881′	0.96	3.80	2.7	Alluvial slit near Toconao, nonsalar
AD04-21	2430	23°59.804′	68°25.320	1.16	−1.82	3.8	Silt, Llano de la Paciencia
AD04-22	2440	23°13.388′	68°33.890′	−1.21	−3.53	4.9	Sand from wash, Llano de la Paciencia
AD04-23	2947	23°07.535′	68°53.833′	−1.62	−3.33	1.3	Eolian from wash bottom, Salar de Laguna Seca
AD04-25	709	23°34.321′	69°50.267′	0.78	−1.89	1.6	Silt, north of Salar de Muerto
AD04-26	705	23°46.514	69°50.267′	3.46	1.22	1.5	Salar de Muerto, dry playa, silt
AD04-27	938	24°03.337′	69°49.469′	−0.27	−4.11	5	Dry playa silt, churned by nitrate mining
AD04-28	1028	24°02.327′	69°52.327′	−0.78	−1.99	1.1	Cerro Moreno, wash silt, drainage all diorite
AD04-29	954	24°04.540′	69°55.437′	3.13	6.16	NA	Phreatic playa, 2 km west of Yungay, subsurface silt
AD04-33	1351	24°13.563′	70°03.781′	3.97	0.20	3.6	Calcareous Av, next to Las Tetas
AD04-35	1907	24°16.550′	70°18.050′	1.51	0.64	1.5	Sag area on hill, Paposo Rd.
AD04-36	2207	24°26.051′	70°19.783′	4.69	0.24	5.3	Calcareous silt from ridge
AD04-38	2092	24°42.556′	70°22.048′	5.28	0.85	4.6	Silt from hillside, sag, along Atacama Fault
AD04-39	128	24°34.090′	70°32.455′	−6.02	−0.83	6.1	Silt peel from Quebrada Iscuna, near Punto del Reyes
AD04-41	932	24°18.641	70°28.657′	1.33	1.54	NA	Silt, small dry playa, Blanco Encalado Rd.
AD04-42	2852	24°11.662′	68°46.865′	−1.80	0.23	3.6	Silt from Imilac salar, phreatic
AD04-43	2877	24°07.689′	68°45.238′	0.57	−4.13	16.4	North end of Imilac salar, phreatic
AD04-47	3311	24°19.182′	68°26.499′	3.45	2.08	2.4	Playa de Inca
AD04-Elvira	2460	23°36.459′	68°48.935′	2.48	−0.56	8.8	Playa Elvira

3.4.2. Oxygen isotopes

$\delta^{18}O$ (VPDB) values of soil carbonate ($\delta^{18}O_{sc}$) coatings and cements in the Atacama range from −5.9‰ to +7.3‰ (Fig. 6; Table 3). The scatter of values with elevation is considerable, but in general, the lowest $\delta^{18}O$ values come from the higher elevations, and the highest values from shallow in soils, and in soils found along the margins of the absolute desert. $\delta^{18}O$ values of carbonate from silty samples in or on the margin of the absolute desert are slightly higher (Table 4; mean = 0.0 ± 3.3‰, $n = 26$) than average soil carbonate values (mean = −1.0 ± 2.7‰).

4. DISCUSSION

4.1. Carbon isotope model

The one-dimensional soil diffusion model developed and tested mainly by Cerling (1984), Quade et al. (1989), and Cerling and Quade (1993) and simplified in Davidson (1995) and Cerling (1999) provides the interpretive context for our results in the Atacama. Here we propose to refine and update the model before applying it to our Atacama soil results. Using the model we can calculate current respiration rates in selected soils.

A number of key assumptions and boundary conditions underpin the original soil diffusion model that are worth restating here, among them the assumption of (1) slow, open-system isotopic exchange of dissolved carbon species with plant-derived CO_2, (2) kinetic enrichment in ^{13}C of soil CO_2 during diffusion, following Stephan–Boltzman's Law, (3) steady-state efflux of CO_2 from the soil, and (4) uniform soil CO_2 production with soil depth. In this paper we focus on revising the production function for CO_2, in light of results from studies of soil CO_2 conducted since 1984.

Evidence points to an exponential, not uniform, decrease in soil CO_2 production (ϕ_s) with soil depth (z) (e.g. Richter, 1987). The general form of this exponential decrease is:

$$\phi_s = \phi_s^0 e^{-z/k} \tag{1a}$$

where k is the characteristic production depth of soil CO_2 and $\phi_s^0 = CO_2$ production rate at the soil surface ($z = 0$).

We can use this information to modify the diffusion model as published thus far. Diffusive transfer of soil CO_2 from the soil to the atmosphere should follow Fick's Second Law, which states that: $\frac{\partial^2 C}{\partial t^2} = D_s \frac{\partial^2 C}{\partial z^2} + \phi_s$

where:

D_s, the diffusion coefficient of CO_2 in soils (cm^2/s) (see Appendix A)
C, CO_2 concentration (in mmole/l)
t, time (s)
z, depth (cm)
ϕ_s, soil CO_2 production (in mmole/cm^2/h)

Soil CO_2 concentrations should be relatively stable (i.e. at steady-state) over the hours to weeks that soil carbonate forms after a rainfall event, such that $\frac{\partial^2 C}{\partial t^2} = 0$, hence:

$$\frac{d^2 C}{dz^2} = -\frac{\phi_s}{D_s} \tag{1b}$$

and the partial differential becomes a simple differential with only two variables remaining. Substitution of Eq. (1a) into Eq. (1b) yields

$$\frac{d^2 C}{dz^2} = -\frac{\phi_s^0 e^{-z/k}}{D_s}$$

We solved this second-order differential equation (fully presented in the Appendix A) to obtain:

$$C_s = \frac{k^2 \phi_s^0}{D_s}(1 - e^{-z/k}) + C_a \tag{2}$$

using several boundary conditions, similar to solutions to the "uniform production" form of the equation (e.g. Cerling, 1984), where C_s and C_a are the concentrations of soil and atmospheric CO_2, respectively. Concentrations of these terms expressed in ppmV can be converted to mmole/l for computational purposes using the Ideal Gas Law.

Davidson (1995) describes the relationship between C_s and other measurable properties in soils as:

$$\delta^{13}C_s = 1.0044\delta^{13}C_{resp} + \frac{C_a}{C_s}(\delta^{13}C_a - 1.0044\delta^{13}C_{resp} - 4.4) + 4.4 \tag{3}$$

where $\delta^{13}C = \left(\frac{R_{sample} - R_{PDB}}{R_{PDB}} - 1\right) \times 1000$, and $R = {}^{13}C/{}^{12}C$, and PDB refers to the PeeDee Belemnite standard, and $\delta^{13}C_{resp}$ refers to the isotopic value of soil-respired CO_2 (the upward flux from the soil).

Substituting Eq. (2) into Eq. (3) and solving for ϕ_s^0 yields:

$$\phi_s^0 = \frac{C_a D_s \left(\left(\frac{\delta^{13}C_a - 1.0044\delta^{13}C_{resp} - 4.4}{\delta^{13}C_s - 1.0044\delta^{13}C_{resp} - 4.4}\right) - 1\right)}{k^2(1 - e^{-\frac{z}{k}})} \tag{4}$$

Soil respiration rates, ϕ_s^0, expressed in Eq. (4) in mmole/cm^3/s, can be converted to a flux (mmole/cm^2/s) across a cross-section 1 cm^2 of soil by multiplying by the production depth, $2k\ln(2)$, and by soil porosity (ε; see Appendix A). In this paper our interest is in calculating ϕ_s^0 from the $\delta^{13}C_{sc}$ values. The temperature-dependent relationship between $\delta^{13}C_{sc}$ and $\delta^{13}C_s$ is expressed as:

$$\delta^{13}C_s = \frac{\delta^{13}C_{sc} + 1000}{\frac{\varepsilon_{sc-s}}{1000} + 1} - 1000 \tag{5}$$

where ε_{sc-s} is the enrichment factor between soil CO_2 and soil carbonate. For ε_{sc-s} we use:

$$\varepsilon_{sc-s} = 11.98(\pm 0.13) - 0.12(\pm 0.1)T\,^{\circ}C \tag{6}$$

from Romanek et al. (1992). Values of $\delta^{13}C_s$ can be calculated from measured $\delta^{13}C_{sc}$ values using Eq. (5) by applying the appropriate soil temperature (in this case mean annual temperature at each site) in Eq. (6). These $\delta^{13}C_s$ values can in turn be substituted into Eq. (4) to obtain an estimate of ϕ_s^0.

4.2. Choice of characteristic production depth (k) for soil CO_2

The key issue for estimating soil respiration rates from $\delta^{13}C_{sc}$ data is the choice of the characteristic production depth for soil CO_2, or k, for the exponential CO_2 production function (Eqs. (1a) and (4)). Year–round measurements of CO_2 with soil depth are not widely available in deserts or elsewhere, forcing us to rely on less direct proxies of CO_2 production. Biotic CO_2 in all soils is produced from both root respiration and microbial oxidation of dead tissue, especially from young, "fast-cycling" soil organic matter (Trumbore, 2000). All root-respired CO_2 and much of the dead tissue (except for leaf litter, a minor term in deserts) in soils should be proportional to overall root biomass. Recent compilations of data on root biomass from 19 desert soils are available in Schenk and Jackson (2002). We fit a simple exponential function to the depth distribution of root biomass in these desert soils and found it has a characteristic production depth of ~32 cm; that is, most CO_2-producing tissue, both live and dead, is in the upper 30 cm of the soil. Some desert plants can root to as deeply as 9 m (Canadell et al., 1996) but a fit to the root biomass distribution with soil depth from Schenk and Jackson (2002) suggests that 98% of production will be captured above a depth of 150 cm in average desert soils.

Previous modeling by us and others assumed CO_2 production uniformly distributed over 1 m of soil depth, with a mean depth of production of 50 cm (e.g. Cerling, 1984; Quade et al., 1989). Soloman and Cerling (1987) correctly pointed out that the form of soil CO_2 production, uniform versus exponentially decreasing, has little effect the resultant $\delta^{13}C_s$ values, as long as the mean production depth does not change. The critical difference for $\delta^{13}C_s$ values in our revised model is that mean production depth is assumed to be significantly shallower, ~22.2 rather than

50 cm. As an example of the effects, this difference in assumed mean production depth increases predicted $\delta^{13}C_s$ values by up to ~0.4‰ in high-respiration rate soils.

4.3. Estimation of the $\delta^{13}C$ value of soil-respired CO_2

Knowledge of the $\delta^{13}C$ value of soil-respired CO_2 ($\delta^{13}C_{resp}$) is required to calculate soil respiration rates in soils (Eq. (4)). In ideal circumstances, the $\delta^{13}C_{resp}$ value is best estimated from soil CO_2 fluxes collected throughout the year. This was not possible given the remoteness of our field area and long transit times back to laboratories in the United States. Instead, we estimated the value of $\delta^{13}C_{resp}$ using the $\delta^{13}C$ value of soil organic matter ($\delta^{13}C_{som}$), and compared it to the $\delta^{13}C$ value of bulk plant matter ($\delta^{13}C_{bulkplant}$), calculated from the $\delta^{13}C$ value of individual plants weighted by their abundance.

Using the $\delta^{13}C$ value of soil organic matter to estimate $\delta^{13}C_{resp}$ has several problems with it. First, soil organic matter may not be well mixed and overrepresent organic matter from single plants nearby. To minimize this effect we amalgamated multiple samples from each site, sieved out coarse organic matter, and ground and homogenized the sieved fractions. Another issue is that, in the course of decay, the $\delta^{13}C$ value of plant tissue can increase in the case of C_3 plants, and decrease in the case of some C_4 plants (Wedin et al., 1995). These combined changes in $\delta^{13}C$ values translate into increases in $\delta^{13}C_{som}$ values with depth in soils (Nadelhoffer and Fry, 1988; Biggs et al., 2002; Biedenbender et al., 2004). To minimize these partially offsetting effects, we confined our sampling to the uppermost 5 cm of soil. Finally, the $\delta^{13}C_{som}$ has likely decreased over past the 150 years in response to decreases of ~1.5‰ (the Suess Effect; Friedli et al., 1986) in the $\delta^{13}C$ value of atmospheric CO_2 ($\delta^{13}C_{atmos.}$) and hence of plant tissue. ^{14}C studies in soils show that these changes only impact the fast-cycling carbon fraction of the soil, a much smaller fraction of bulk soil organic matter than the unaffected slow-cycling fraction (Trumbore, 2000). The impact of changes in the $\delta^{13}C_{atmos.}$ on $\delta^{13}C_{som}$ values is strongly dependent on the residence time of bulk organic matter in soils, which studies in desert soils indicate is >150 yrs (Connin et al., 1997). Assuming a residence time of ~215 years from Connin et al. (1997), the average decrease in $\delta^{13}C_{som}$ in Atacama soils over the past 215 years is a modest ~0.36‰ (Fig. 7). We adjust the $\delta^{13}C_{som}$ values by this amount in estimating soil respiration rates later in the paper.

$\delta^{13}C_{bulkplant}$ values do not correlate well with $\delta^{13}C_{som}$ values (Fig. 8). This could be the result of several factors. To make the comparison with adjusted $\delta^{13}C_{som}$ values, we must add 1.5‰ (Suess Effect) to $\delta^{13}C_{bulkplant}$ values due to the equivalent shift in $\delta^{13}C_{atmos.}$ values. First, the contribution of individual plants to $\delta^{13}C_{resp.}$ should be proportional to that plant's overall biomass, not the area the plant covers above ground, as measured by our surveys. Second, $\delta^{13}C$ values can vary across an individual plant by several per mil; we only measured the biotically most active above-ground tissues of plants, their leaves or green stems. Third, the extent and composition of plant cover varies during the year, given the seasonal and highly intermittent nature of rainfall at most sites. This biases our measurements against small annuals, which dry up and blow away from the sites.

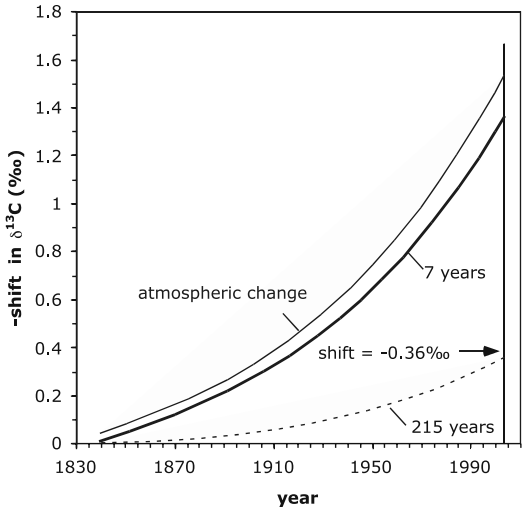

Fig. 7. Modeled $\delta^{13}C$ (VPDB) value of soil organic matter at different soil organic turnover times, compared to the $\delta^{13}C$ (VPDB) value of atmospheric CO_2 since 1840 given in Friedli et al. (1986).

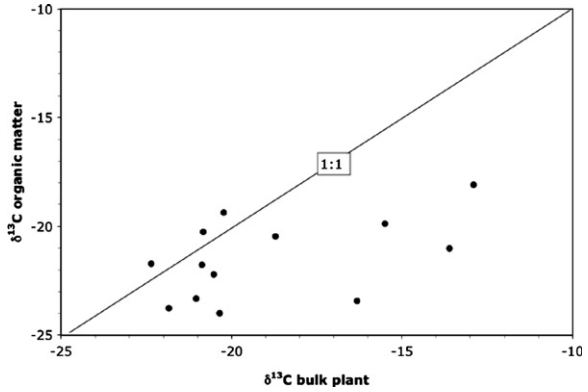

Fig. 8. $\delta^{13}C$ (VPDB) value of soil organic matter versus $\delta^{13}C$ (VPDB) estimated from weighted plant proportions at each site.

Estimated $\delta^{13}C_{bulkplant}$ values tend to be higher than $\delta^{13}C_{som}$ values (Fig. 8). During our plant survey we noted the presence of many dried, sometimes fragmented herbaceous annuals in varying stages of being blown clear of the sites. Most of these annuals are C_3 plants, which would explain why most estimated $\delta^{13}C_{bulkplant}$ values tend to be higher than $\delta^{13}C_{som}$ values. Hence, readers should be aware that our plant surveys in Table 2 probably provide a reasonable picture of woody perennial species but tend to under represent the annuals.

4.4. The $\delta^{13}C$ record from soil carbonates

$\delta^{13}C_{sc}$ values from recent (Stage I–II) soil carbonate show weak trends with elevation (Fig. 5), unlike soil carbonates from the Mojave Desert (Amundson et al., 1988; Quade et al., 1989), and display significant within site scatter. The general pattern is that $\delta^{13}C_{sc}$ values are lowest on

the most coastal portion of the Paposo transect and highest on the Socompa transect (Fig. 5). Qualitatively, this can be explained by more moisture (indicative of higher respiration rates) and the dominance of C_3 plants on the Paposo transect, contrasted with more C_4 plants and much drier conditions on the Socompa transect. Perhaps the most striking results are the very high $\delta^{13}C_{sc}$ values from sites bordering and in the absolute desert, even from depths below 30 cm. We attribute this to the very low rainfall (and low respiration rates) at these sites, and not to the nature of the plant cover, which is sparse to absent, and where present includes few C_4 plants.

We attribute the weak correlation of $\delta^{13}C_{sc}$ values with elevation to several causes (1) the attenuated isotopic difference between C_3 and C_4 plants of only 8–9‰, in contrast to global average differences closer to 13–14‰, (2) small contrasts in $\delta^{13}C_{som}$ between sites, falling in the −18 to −26‰ range, and (3) possibly strong seasonal and intra-annual variations in rainfall and therefore respiration rates.

4.5. Modeled soil respiration rates

We are now positioned to quantitatively examine the relative contribution of respiration rates and C_3/C_4 plant proportions to $\delta^{13}C_{sc}$ values, and to relate these conclusions to other soil parameters such as % organic C in soils. Our estimates for soil respiration rates assume:

(1) $\delta^{13}C_{resp} = \delta^{13}C_{som}$, after correcting for the Suess Effect by adding 0.36‰ to $\delta^{13}C_{som}$
(2) k (1/e folding depth) = 32 cm
(3) porosity = 0.5
(4) the temperature (Table 1) and pressure (Appendix A) specific to each site
(5) specified soil sampling depths
(6) soil carbonate formed in the presence of vegetation similar to today's.

Modeled respiration rates vary between 1.8 and 3.7 mmole/m^2/h at in the foggy lower coastal Lomas zone, to rates around 0 at sites on the lower (Table 2c: Paposo 1240 and 1460 m) and upper (Socompa 3123 m) fringes of the absolute desert. Between these extremes, respiration rates are much higher on the wetter Paso de Jama (Table 2a) than the arid Socompa transect sites (Table 2b).

Several simple comparisons demonstrate the dominance of respiration rates in determining $\delta^{13}C_{sc}$ values (Figs. 9a and b). $\delta^{13}C_{sc}$ values decline exponentially with respect to modeled respiration rates (Fig. 9a; solid circles), following the generally predicted negative exponential relationship (Fig. 9a; line) between the two parameters for "average" (see Fig. 9a caption) soil conditions in our study area. The fit of modeled and observed values is slightly better if only sites with C_3 biomass are considered (Fig. 9a). Not surprisingly, $\delta^{13}C_{sc}$ values also decrease exponentially with % organic C in surface A horizons (Fig. 9b), another measure of soil organic productivity.

There is a tendency in much of the soils and speleothem isotopic literature to ignore the influence of respiration rates on $\delta^{13}C_{sc}$ values. This is warranted where respiration rates are high, whereas in deserts it should always be taken into account. The contribution of atmospheric CO_2 to $\delta^{13}C_{sc}$ values at and below 50 cm soil depth is apparent (Fig. 10) in our study sites where rainfall/fog drip is <10 cm/year.

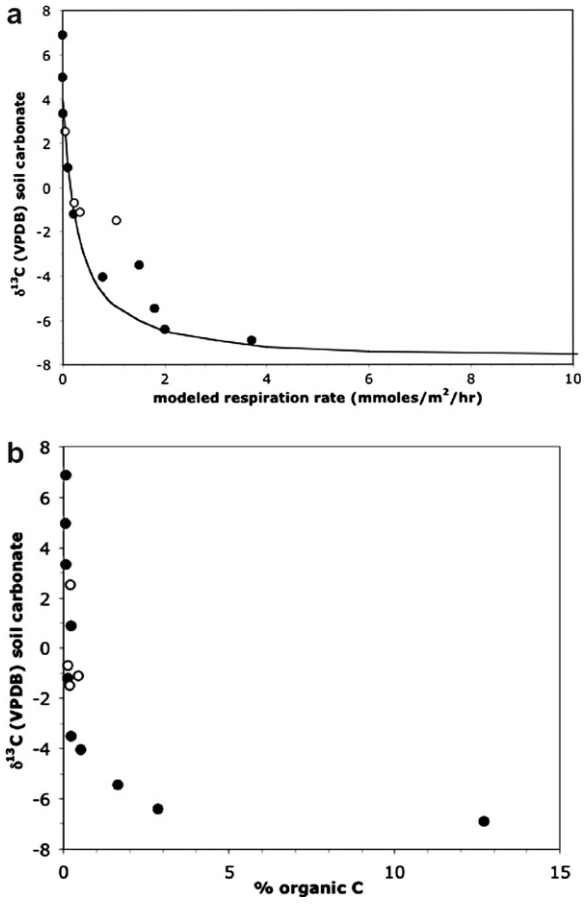

Fig. 9. $\delta^{13}C$ (VPDB) of soil carbonate versus (a) modeled respiration rates for each site and generalized model respiration rates (black line) assuming "average" transect site conditions of $T = 9$ °C, $\delta^{13}C_{resp.} = -23‰$, $\delta^{13}C_a = -6.5‰$, elevation = 1000 m, k (characteristic production depth) = 32 cm, (b) per cent carbon in surface A horizons. Solid circles: C_3 plants >75%; open circles: C_4 + CAM plants = 42–100%.

4.6. Carbonate in the absolute desert: biotic or abiotic?

The trace quantities of fine-grained carbonate in soils from the absolute desert formed either from *in situ* weathering, or represent detrital material washed or blown into the site. If formed *in situ*, the high average $\delta^{13}C_{sc}$ values of +4.1‰ suggest carbonate formation at isotopic equilibrium with pure atmospheric CO_2, assuming soil temperatures between 12 and 18 °C. Our soil samples come from ~5 to 40 cm, pointing to purely atmospheric origin even deep in the profile. Alternatively, carbonate many be detrital, and represent carbonate formed in some other setting. This is possible since carbonate is present in trace amounts all through the area, in dry washes and on playas (Table 3), and could plausibly be mixed with alluvial parent material. The main

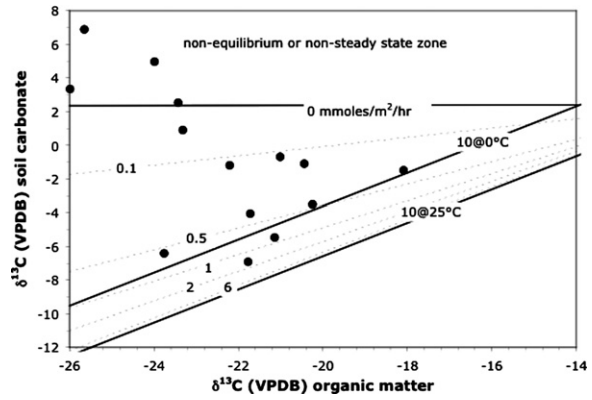

Fig. 10. $\delta^{13}C$ (VPDB) of soil carbonate versus $\delta^{13}C$ (VPDB) of soil organic matter from Atacama soils. The lower two solid lines represent modeled isotopic values defining high respiration-rate soils (10 mmole/m^2/h) between 0 and 25 °C. The dashed lines represent a range of soil respiration rates (numbers) calculated at 25 °C only. Solid circles are observed values at transect sites. These mostly plot above the field defined for high respiration-rate soils, reflecting the influence of atmospheric CO_2.

problem with this explanation is that surficial silt displays much lower average $\delta^{13}C$ values of +1.3‰ than carbonates in the soils (Table 3). Hence we favor the idea that carbonate in the absolute desert soils formed *in situ* in the presence of pure atmospheric CO_2, with no evidence of a contribution from plant CO_2 at any depth. This interesting result means that vascular plant life leaves a clear isotopic imprint on soil carbonate values, even where plant cover is extremely sparse. It also suggests that carbonate—albeit in trace amounts—can form even where no life is visible on the surface. It is important to keep in mind, however, that absolute desert soils may be plantless but they are not lifeless. Our results do not preclude the possibility that microscopic life plays some role in this carbonate formation, but without leaving any isotopic imprint, since traces of microbial life have been identified at depth in all our absolute desert study soils (Maier et al., 2004; Drees et al., 2006).

4.6.1. Evidence for paleoenvironmental change

$\delta^{13}C_{sc}$ values are potential archives of vegetation and climate change in the past, especially in carbonate deeper than 50 cm, where the influence of atmospheric CO_2 is minimized and changes in the contribution of plant CO_2 are more visible. We sampled soil carbonates from mature surface paleosols (Stage III–IV), in addition to the weakly developed (Stage I–II) carbonates already reported above. $\delta^{13}C_{sc}$ values in these two age groupings (Stage I–II versus Stage III–IV) from >50 cm soil depth do not show systematic differences (Table 3). The strong overlap in the isotopic values of the two groupings suggest that changes in the isotopic composition of average soil CO_2 at most sites has not changed significantly over the latter part of the Quaternary.

This is not to say that vegetation has not shifted with time in response to climate change in the Atacama, changes readily visible in the fossil rodent midden and other records from the region (e.g. Veit, 1993; Grosjean and Núñez, 1994; Rech et al., 2003). For example, midden records show a downslope displacement at least by 500–800 m of species from higher vegetation belts during the last major wet phase in the region 9500 to 13,800 calendar years BP (Latorre et al., 2002). Thus, in the area now covered by *Atriplex* and *Artemisia* Tolar, species from the high Andean steppe grassland were also present. Average $\delta^{13}C_{om}$ values in these two zones differ by about 3–5‰, large enough to be visible in $\delta^{13}C_{sc}$ values. This may be the explanation for the distinctly different $\delta^{13}C_{sc}$ values seen in buried paleosols from the Pampa de Inca site at 3305 m on the Socompa transect (Figs. 2b and Fig. 11a; Table 2c). This buried soil complex is developed in alluvial fan gravel and sand derived from local ignimbrites. $\delta^{13}C_{sc}$ values in the upper paleosol are more positive (>−1.5‰) than those (<−1.5‰) in the underlying paleosol, a difference attributable to formation under modern cover with abundant *Atriplex* for the upper paleosol and under high Andean steppe for the lower paleosol. $\delta^{18}O_{sc}$ values also differ between profiles (Fig. 11b), consistent with less evaporation or cooler temperatures of formation in the lower profile, as discussed in Section 4.7.

Another zone that might experience the detectable isotopic effects of vegetation change is the currently unvegetated fringes of the absolute desert. We sampled a soil profile on one such setting east of San Pedro de Atacama at 2445 m (Fig. 2a: LP 2445), located only a few hundred meters below the current vegetation limit. Because today the area is unvegetated, the profile might be expected to produce soil carbonate in isotopic equilibrium with atmospheric values (~4.0‰), as already discussed. Instead $\delta^{13}C_{sc}$ values drop as low as −1‰ with soil depth, firm evidence that plants once grew at the site (Table 2c; Fig. 11b). The age of the carbonate is unknown but may have formed in the presence of Tolar and prepuna shrubs that likely descended to this elevation between 9500 and 13,800 calendar years BP.

4.7. The $\delta^{18}O$ record

The general pattern in $\delta^{18}O_{sc}$ values in the Atacama soils (Fig. 6) can be understood in terms of the three variables that likely determine the $\delta^{18}O$ value of most soil carbonate: the $\delta^{18}O$ value of local meteoric water, soil temperature, and the extent of evaporation of soil water prior to soil carbonate formation. By comparing to weakly developed carbonate (Stage I–II) formed in climate conditions similar to today's, we can use modern soil temperature and $\delta^{18}O$ values of rainfall ($\delta^{18}O_{mw}$) to reconstruct the extent of soil dewatering prior to soil carbonate formation.

4.7.1. $\delta^{18}O$ value of meteoric water and soil temperature

$\delta^{18}O_{mw}$ data are available from two studies (Fritz et al., 1981; Aravena et al., 1999). These data are weighted by rainfall amount, and are strongly skewed toward summer rainfall, which at higher elevations constitutes ~80% of annual rainfall. The relationship ($r^2 = 0.60$) between $\delta^{18}O_{mw}$ and elevation above 2500 m can be described by:

$$\text{elevation (masl)} = -7.7257(\delta^{18}O_{mw})^2 - 289.4(\delta^{18}O_{mw}) + 1376.6 \quad (7)$$

$\delta^{18}O$ values for fog and Pacific rainfall in the coastal zone (<1000 m) collected by Aravena et al. (1989) show little

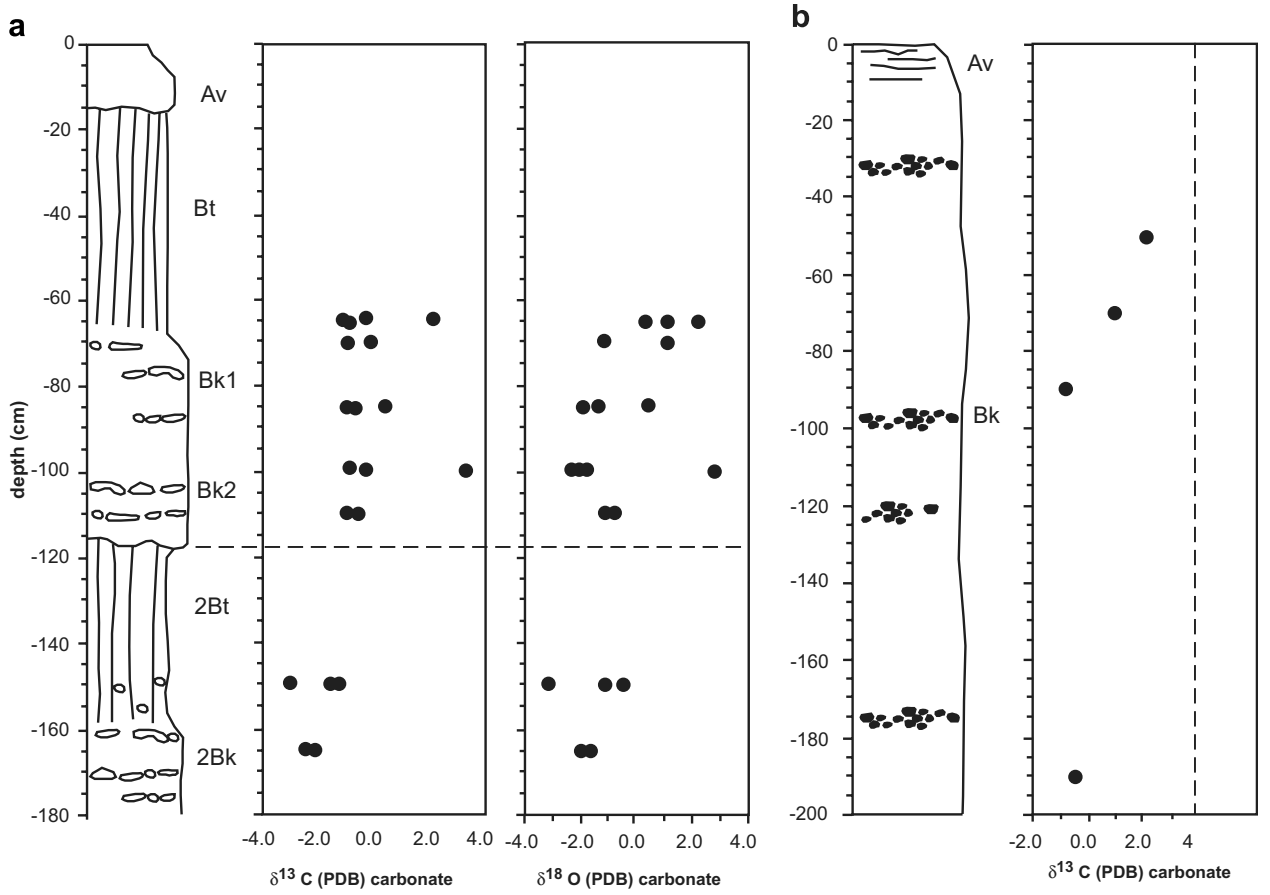

Fig. 11. (a) Profile, $\delta^{13}C$ (VPDB), and $\delta^{18}O$ (VPDB) values of soil carbonate versus depth from Pampa de Inca (Soc 3305 m; see Fig. 2b), horizontal dashed line divides upper and lower paleosols; (b) $\delta^{13}C$ (VPDB) of soil carbonate versus depth from Llano de la Paciencia 2445 m (see Fig. 2a: LP2445). Vertical dashed line denotes $\delta^{13}C_{sc}$ value formed in equilibrium with the atmosphere.

variation and average -1.87 ± 0.67 and $-5.55 \pm 0.73‰$, respectively. We adopt this set of values to predict $\delta^{18}O$ (VPDB) values for soil carbonate.

We can predict the mean and range of $\delta^{18}O$ values for soil carbonate at each site, assuming the fractionation factor (α) between calcite and water of $1000 \ln \alpha_{calcite-water} = (18{,}030/T) - 32.42$, where T is in K (Kim and O'Neil, 1997). We assume mean annual air temperatures. All observed $\delta^{18}O$ values are higher (up to 10‰) than values predicted to be in equilibrium with local rainfall, and in the case of the coastal zone (Fig. 6), with fog drip as well. This pattern suggests that soils undergo significant dewatering by evaporation prior to carbonate formation, an effect that we quantify next.

4.7.2. Evaporation

We can model the minimum dewatering loss of soils by evaporation prior to carbonate formation using simple Rayleigh fractionation:

$$\delta^{18}O_{finalwater} = (\delta^{18}O_{initial} + 1000) f^{\alpha_T - 1} - 1000$$

where

f is fraction of original liquid water left in soil,
$\alpha_T = \alpha_{v-l} + 14.2\,(1 - h)/1000$,
α_{v-l} is the equilibrium fractionation factor between vapor and liquid (adjusted for local soil T) and h (expressed as a fraction) is humidity in the soil pore space.

Assuming an end-member case of $h = 1$ (humidity = 100%), the fraction of water remaining prior to carbonate formation in transect soils varies between 0.9 and 0.1. Use of lower humidity reduces the estimate of fraction lost. The most extreme dewatering by evaporation occurs in soils on the dry upper Socompa transect (0.5–0.1); the least occurs in soils from the wetter Paposo ($f = 0.9$–0.4) transect. Calama transect soils are intermediate ($f = 0.8$–0.3) in terms of evaporation of soil water, matching the intermediate levels of rainfall.

In the Lomas zone we calculated the $\delta^{18}O_{sc}$ value formed in equilibrium with both rainfall derived from Pacific storms and from fog drip. As with the rest of the transect, all of the soil carbonates in this zone returned $\delta^{18}O$ values higher than the value predicted to form in equilibrium with $\delta^{18}O_{mw}$ values (in this case from Pacific storms), as well fog drip. Because of these evaporation effects, it is not possible to establish the proportions that fog drip and rainfall contribute to Lomas soils.

The $\delta^{18}O_{sc}$ value of paleosol carbonates is increasingly used in paleoelevation reconstruction (e.g. Garzione et al.,

2000; Currie et al., 2005). For example, in our study area the $\delta^{18}O_{mw}$ value of rainfall varies strongly between 3800 and 2500 m, where it decreases by about −6‰/km ($r^2 = 0.6$). Such relationships have been used as a basis for paleoelevation reconstruction, using paleosol $\delta^{18}O_{sc}$ values assumed to form in isotopic equilibrium with waters of elevation-dependent composition. However, few systematic studies of variation of $\delta^{18}O_{sc}$ values themselves (as opposed to natural waters) with elevation have been conducted. In hyperarid settings such as the Atacama, the overprinting effects of evaporation clearly overwhelm any potentially useful relationship between $\delta^{18}O_{sc}$ values and elevation (Fig. 6).

4.8. Comparison to the isotopic record of soil carbonates in other deserts

A compilation of published and unpublished isotopic results (Fig. 12) from soil carbonate (depths largely >50 cm) from many of the world's deserts reveals some interesting patterns. $\delta^{13}C_{sc}$ values from all deserts range from −10.4‰ to +8.2‰. Carbonate from the Atacama and Mojave display a similar wide range in $\delta^{13}C_{sc}$ values. Some of this wide range is an artifact of variable carbonate distribution with depth. Carbonate in both the Mojave and Atacama Deserts precipitates right up to the soil surface, a result of the aridity of both deserts.

Elevated $\delta^{13}C_{sc}$ values of +4.0‰ to +7.9‰ tend to occur at very shallow soil depths in the Atacama, values higher than predicted for formation at isotopic equilibrium with the atmosphere (Fig. 10). Such anomalous $\delta^{13}C_{sc}$ values are known from several other slightly unusual surficial contexts, possibly providing clues as to their origin. One is from carbonate collars forming around surface stones interlocked into desert pavements in the Monte Desert in Argentina and the Mojave Desert (McFadden et al., 1998). A second context is in fractures or vugs from relatively unvegetated basalt flows (Knauth et al., 2003). What these sites and those in the Atacama and Mojave have in common are sparse vegetation cover, a surface context in some cases, and in other cases a relatively open, porous soil structure in gravels or fractured, vuggy basalt, and high $\delta^{18}O_{sc}$ values.

Rapid loss of CO_2, possibly through advection of soil air near the soil surface and at depth along burrows and fractures, is the most plausible explanation for the elevated $\delta^{13}C_{sc}$ values observed in and outside the Atacama Desert. Advection is known to occur shallow in soils in response to barometric pressure changes (Buckingham, 1904). Such rapid loss of CO_2 could produce isotopic disequilibrium, particularly affecting the back-reaction of gaseous CO_2 with dissolved HCO_3^-. The reaction is kinetically slow and is thought to contribute to the significant enrichments in $\delta^{13}C_{sc}$ and $\delta^{18}O_{sc}$ observed in cave speleothems and spring travertines, as water off-gases CO_2 into the lower pCO_2 environment (e.g. Fantidis and Ehhalt, 1970; Dulinski and Rozanski, 1990; Mickler et al., 2006).

$\delta^{18}O_{sc}$ values from the Atacama are also markedly higher than any other desert in the world (Fig. 12). High $\delta^{18}O_{mw}$ values are not the cause of this, because $\delta^{18}O_{mw}$ values from the Atacama Desert are as low or lower than most other comparison deserts. When we plot observed versus predicted $\delta^{18}O_{sc}$ values (assuming mean annual T) from three major deserts, the driest settings, Death Valley, USA, and the Atacama sites, plot furthest from the 1:1 line (Fig. 13). This pattern must be the result of extreme evaporation due to the hyperaridity.

5. CONCLUSIONS

C_3 plants dominate the flora of the central sector of the Atacama Desert, especially in the coastal fog zone, and C_4 plants, where present, are mainly the shrub *Atriplex*

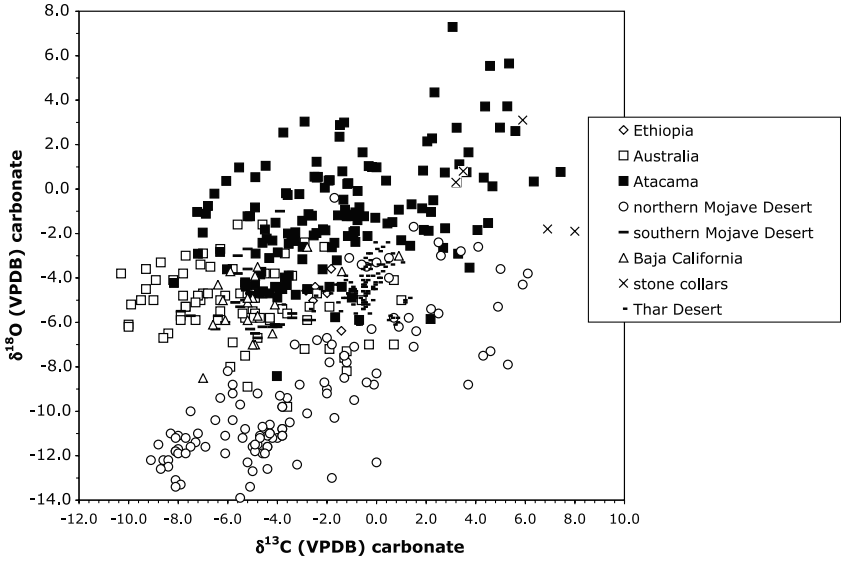

Fig. 12. $\delta^{13}C$ (VPDB) versus $\delta^{18}O$ (VPDB) value of soil carbonate from deserts globally. Sources: northern Mojave Desert (Quade et al., 1989); southern Mojave Desert (Liu et al., 1996); Australia (Quade, unpub data); Ethiopia (Quade, unpub. data); Thar Desert (Achyuthan et al., 2007); Baja California (Amundson et al., 1994); stone collars (McFadden et al., 1998).

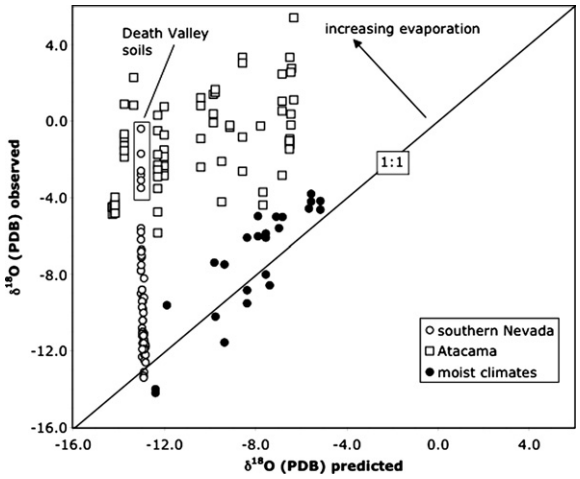

Fig. 13. The $\delta^{18}O_{cc}$ (observed) (data from Cerling and Quade (1993), Quade et al. (1989), and this paper) versus predicted $\delta^{18}O_{cc}$ values based on local mean annual temperature and $\delta^{18}O_{mw}$ values of local rainfall.

imbricata. $\delta^{13}C_{sc}$ values vary between −8.2‰ at the wettest sites and +7.9‰ at the driest. The lowest values come from the relatively moist coastal lomas and reflect high respiration rates and high proportions of C_3 plants. The highest $\delta^{13}C_{sc}$ values come from the margins and core of the absolute desert or from the very dry Socompa transect sites. We used Suess Effect corrected-$\delta^{13}C$ values of soil organic matter as a proxy for plant respiratory $\delta^{13}C$ values, and applied them toward calculating soil respiration rates at a number of sites, using the soil diffusion model of Cerling (1984). We modified that model by incorporating a more realistic, exponentially decreasing soil CO_2 production function with depth. Assuming relatively shallow characteristic production depths (~32 cm) for that function, we calculated soil respiration rates between virtually zero on the fringes of the absolute desert to ⩽4 mmole/m^2/h in the fog drip-dominated coastal lomas. Not surprisingly, modeled soil respiration rates are strongly correlated with measured % organic carbon in soils. Trace carbonates from the absolute desert formed in equilibrium with pure atmosphere, consistent with the total absence of plants in that zone, and pointing to a probable abiotic origin.

$\delta^{18}O_{sc}$ values vary between −8.4‰ at the wettest sites and +7.3‰ at the driest. All samples at all sites, including in the fog-dominated coastal areas, show the effects of moderate to strong evaporation of soil water prior to carbonate formation. These evaporation effects are the strongest of any desert in the world, commensurate with the hyperaridity of the Atacama, past and present.

ACKNOWLEDGMENTS

We thank Brian Enquist and Thure Cerling for discussions, Camille Holmgren for assistance with climate data, and Mike Dillon for help with identification of plants in the Lomas. We also thank Ron Amundson, associate editor Stephan Kraemer, and two anonymous reviewers for their highly constructive feedback. This research was supported largely by the National Geographic Society, with additional support from NSF 02-13657 to J.Q. and J.B. C.L. acknowledges support from FONDECYT 3030062 and from FONDAP-FONDECYT 1501-0001 to the Center for Advanced Studies in Ecology & Biodiversity. C.L. and M.T.K. also acknowledge ongoing support from ICM grant P02-051-FICM.

APPENDIX A

A.1. Solution to the differential equation

$$\frac{d^2C}{dz^2} = -\frac{\phi_s^0 e^{-z/k}}{D_s} \tag{A.1}$$

define:

$$J_s = -D_s \frac{dC}{dz} \tag{A.2}$$

substitute (A.2) into (A.1)

$$\frac{dJ_s}{dz} = \phi_s^0 e^{-z/k}$$

and integrate:

$$\int_0^{\phi_s} d\phi_s = \phi_s^0 \int_L^z e^{-z/k}\, dz$$

$$J_s = -k\phi_s^0 (e^{-z/k} - e^{-L/k}) \tag{A.3}$$

substitute (A.3) into (A.2):

$$\frac{dC}{dz} = \frac{k\phi_s^0}{D_s}(e^{-z/k} - e^{-L/k})$$

and integrate:

$$\int_{C_a}^{C_s} dC = \frac{k\phi_s^0}{D_s} \int_0^z (e^{-z/k} - e^{-L/k})\, dz$$

$$C_s - C_a = \frac{k\phi_s^0}{D_s}(-ke^{-z/k} + k - ze^{-L/k})$$

which is the solution for the definite integral, but as $L \to \infty$, $ze^{-L/k} \to 0$, hence, for the solution to the indefinite integral (i.e. infinite soil depth):

$$C_s - C_a = \frac{k\phi_s^0}{D_s}(-ke^{-z/k} + k)$$

or:

$$C_s = \frac{k^2\phi_s^0}{D_s}(1 - e^{-z/k}) + C_a$$

A.2. Diffusion coefficient in soil

The diffusion coefficient for soils (D_s) is related to that in air (D_{air}) in units of cm^2/s by:

$$D_s = D_{air}\varepsilon\rho$$

where ε is soil porosity, and ρ is a soil pore tortuosity (both terms are unitless). In this paper we assume values of 0.5 and 0.6 for each term, respectively. D_{air} must be corrected for pressure (as a function of elevation) and temperature following:

$$D_{\text{air}} = D^0_{\text{air}} \left[\left(\frac{P_0}{P} \right) \left(\frac{T}{T_0} \right) \right]^{1.823}$$

where D^0_{air} is the diffusion coefficient in air at 1 atm and 298 K, P_0 and T_0 are 1 atm and 273.15 K, and P and T are temperature (in Kelvins) and ambient pressure (in atm) at the soil site. Ambient pressure at each soil site can be calculated from:

$$P_{\text{air}} = \left(\frac{T(\text{K}) - 0.0065 * \text{elevation}}{T(\text{K})} \right)^{5.257}$$

A.3. Mean production depth

The production depth for soil CO_2 that decreases exponentially with soil depth (z) is assumed to be twice the mean production depth. The mean production depth (z_{mean}) in a soil where the characteristic production depth (1/e-folding depth), k, is:

$$0.5 = e^{-z_{\text{mean}}/k} \text{ or}$$

$$z_{\text{mean}} = k \ln(2)$$

the total production depth is $2 * z_{\text{mean}}$.

REFERENCES

Achyuthan H., Quade J., Placzek C. and Roe L. J. (2007) Stable isotopic composition of pedogenic carbonates from the eastern margin of the Thar Desert, Rajasthan, India. *Quaternary International* **162–163**, 50–60.

Amundson R. G., Chadwick O. A., Sowers J. M. and Doner H. E. (1988) The relationship between modern climate and vegetation and the stable isotope chemistry of Mojave Desert soils. *Quaternary Res.* **29**, 245–254.

Amundson R., Franco-Vizcaino E., Graham R. C. and DeNiro M. (1994) The relationship of precipitation seasonality, flora and stable isotope chemistry of soils in the Vizcaino desert, Baja California, Mexico. *J. Arid Environ.* **28**, 265–279.

Aravena R., Suzuki O. and Pollastri A. (1989) Coastal fog and its relation to groundwater in IV region of northern Chile. *Chem. Geol. (Isot. Geos. Sec.)* **79**, 83–91.

Aravena R., Suzuki O., Pena H., Pollastri A., Fuenzalida H. and Grilli A. (1999) Isotopic composition and origin of precipitation in northern Chile. *Appl. Geochem.* **14**, 411–422.

Arroyo M. T. K., Squeo F. A., Armesto J. J. and Villagran C. (1988) Effects of aridity on plant diversity in the northern Chilean Andes: results of a natural experiment. *Ann. Missouri Botanical Garden* **75**, 55–78.

Banfield J. L., Glotch T. M. and Christensen P. R. (2003) Spectroscopic identification of carbonate minerals in Martian dust. *Science* **301**, 1084–1087.

Berger I. A. and Cooke R. U. (1997) The origin and distribution of salts on alluvial fans in the Atacama Desert, northern Chile. *Earth Surf. Process. Landforms* **22**, 581–600.

Betancourt J. L., Latorre C., Rech J. A., Quade J. and Rylander K. A. (2000) A 22,000 year record of monsoonal precipitation from northern Chile's Atacama Desert. *Science* **289**, 1542–1546.

Biedenbender S., McClaran M., Quade J. and Weltz M. A. (2004) Landscape patterns of vegetation change indicated by soil isotope composition. *Geoderma* **119**, 69–83.

Biggs T., Quade J. and Webb R. H. (2002) The $\delta^{13}C$ value of soil organic matter in a semi-arid grassland with mesquite (Prosopis) encroachment in southeast Arizona. *Geoderma* **110**, 109–130.

Buckingham E. (1904) Contributions to our knowledge of the aeration of soils. Bulletin 25. USDA Bureau of Soils, Washington, DC.

Canadell J., Jackson R. B., Ehleringer J. R., Mooney H. A., Sala O. E. and Schulze E.-D. (1996) Maximum rooting depth of vegetation types at the global scale. *Oecologia* **108**, 583–595.

Cereceda P., Osses P., Larrain H., Farias M., Lagos M., Pinot R. and Schemenauer R. S. (2002) Advective, orographic, and radiation fog in the Tarapaca region, Chile. *Atmos. Res.* **64**, 261–271.

Cerling T. E. (1984) The stable isotopic composition of modern soil carbonate and its relation to climate. *Earth Planet. Sci. Lett.* **71**, 229–240.

Cerling T. E. (1999) Stable isotopes in paleosol carbonates. In *Palaeoweathering, Palaeosurfaces, and Related Continental Deposits*, vol. 27 (eds. M. Thiry and R. Simon-Coincon). Oxford International Association of Sedimentologists Special Publication, pp. 43–60.

Cerling T. E. and Quade J. (1993) Stable carbon and oxygen isotopes in soil carbonates. In *Continental Indicators of Climate*, vol. 78 (eds. P. Swart, J. A. McKenzie and K. C. Lohman). Proceedings of Chapman Conference, Jackson Hole, Wyoming, American Geophysical Union Monograph, pp. 217–231.

Connin S. L., Virginia R. A. and Chamberlain C. P. (1997) Carbon isotopes reveal soil organic matter dynamics following arid shrub expansion. *Oecologia* **110**, 374–386.

Currie B. S., Rowley D. B. and Tabor N. J. (2005) Middle Miocene paleoaltimetry of southern Tibet: implications for the role of mantle thickening and delamination in the Himalayan orogen. *Geology* **33**(3), 181–184.

Davidson G. R. (1995) The stable isotopic composition and measurement of carbon in soil CO_2. *Geochim. Cosmochim. Acta* **59**(12), 2485–2489.

Drees K. P., Neilson J. W., Betancourt J. L., Quade J., Henderson D. A., Pryor B. M. and Maier R. M. (2006) Bacterial community structure in the hyperarid core of the Atacama Desert, Chile. *Appl. Environ. Microbiol.* **72**(12), 7902–7908.

Dulinski M. and Rozanski K. (1990) Formation of $^{13}C/^{12}C$ isotopic ratios in speleothems: a semi-dynamic model. *Radiocarbon* **32**, 7–16.

Ehleringer J. R. (1988) Carbon isotope ratios and physiological processes in aridland plants. In *Symposium Proceedings: Applications of Stable Isotope Ratios to Ecological Research* (eds. P. W. Rundel, J. R. Ehleringer, and K. A. Nagy). Springer, New York, pp. 41–54.

Ericksen G. E. (1981) Geology and origin of the Chilean nitrate deposits. U.S. Geological Survey Professional Paper 1188, 37pp.

Fantidis J. and Ehhalt D. H. (1970) Variations of the carbon and oxygen isotopic composition of stalagmites and stalagtites; evidence of non-equilibrium isotopic fractionation. *Earth Planet. Sci. Lett.* **10**, 136–144.

Fox D. and Koch P. L. (2004) Carbon and oxygen isotopic variability in Neogene paleosol carbonates: constraints on the evolution of C_4 grasslands. *Palaeogr. Palaeocl. Palaeoecol.* **207**, 305–329.

Friedli H., Lotscher H., Oeshger H., Siegenthaler U. and Stauffer B. (1986) Ice core record of the $^{13}C/^{12}C$ ratio of atmospheric CO_2 in the past two centuries. *Nature* **324**, 237–238.

Fritz P., Suzuki O., Silva C. and Salati E. (1981) Isotope hydrology of groundwater in the Pampa del Tamarugal, Chile. *J. Hydrol.* **53**, 161–184.

Garreaud R. D. (1999) Multiscale analysis of the summertime precipitation over the central Andes. *Monthly Weather Rev.* **127**, 901–921.

Garzione C. N., Quade J., DeCelles P. G. and English N. B. (2000) Predicting paleoelevation of Tibet and the Himalaya from $\delta^{18}O$ versus altitude gradients in meteoric water across the Nepal Himalaya. *Earth Planet. Sci. Lett.* **183**, 215–229.

Gibson E. K., et al. (2001) Life on Mars: evaluation of the evidence within Martian meteorites ALH84001, Nakhla, and Shergotty. *Precambrian Research* **106**, 15–24.

Gile L. H., Peterson F. F. and Grossman R. B. (1966) Morphological and genetic sequences of carbonate accumulation in desert soils. *Soil Sci.* **101**, 347–360.

Grosjean M. and Núñez L. A. (1994) Lateglacial, early and middle Holocene environments, human occupation, and resource use in the Atacama (northern Chile). *Geoarcheology* **9**(4), 271–286.

Houston J. and Hartley A. J. (2003) The central Andean west – slope rainshadow and its potential contribution to the origin of hyperaridity in the Atacama Desert. *Int. J. Climatol.* **23**, 1453–1464.

Kim S.-T. and O'Neil J. R. (1997) Equilibrium and non-equilibrium oxygen isotope effects in synthetic carbonates. *Geochim. Cosmochim. Acta* **61**, 3461–3475.

Knauth P., Brilli M. and Klonowski S. (2003) Isotope geochemistry of caliche developed on basalt. *Geochim. Cosmochim. Acta* **67**(2), 185–195.

Larrain H., Velazquez F., Cereceda P., Espejo R., Pinot R., Osses P. and Schemenauer R. S. (2002) Fog measurements at the site "Falde Verde" north of Chanaral compared with other fog stations of Chile. *Atmos. Res.* **64**, 273–284.

Latorre C., Betancourt J., Rylander K. and Quade J. (2002) Vegetation invasions into the absolute desert: a 45,000 yr rodent midden record from the Calama-Salar de Atacama basins, northern Chile (lat22°–24°S). *Geol. Soc. Am. Bull.* **114**(3), 349–366.

Latorre C., Betancourt J., Rech J., Quade J., Holmgren C., Plazcek C., Maldonado A., Vuille M. and Rylander K. (2005) Late Quaternary history of the Atacama Desert. In *Archeology and Environmental History of the Southern Deserts* (eds. M. Smith and P. Hesse). National Museum of Australia Press, Canberra, pp. 73–90.

Liu B., Phillips F. M. and Campbell A. R. (1996) Stable carbon and oxygen isotopes of pedogenic carbonates, Ajo Mountains, southern Arizona: implications for paleoenvironmental change. *Palaeogeogr., Palaeoclim., Palaeoecol.* **124**, 233–246.

Machette M. A. (1985) Calcic soils of the southwestern United States. In *Soils and Quaternary geology of the southwestern United States* (eds. D. L. Weide and M. L. Faber). Geol. Soc. Am. Spec. Pap., vol. 203, pp. 1–21.

Maier R. M., Drees K. P., Neilson J. W., Henderson D. A., Quade J. and Betancourt J. (2004) Letters to Editor: Microbial life in the Atacama Desert. *Science* **306**, 1289.

McAuliffe J. R. (1991) A rapid survey method for estimation of density and cover in desert plant communities. *J. Veg. Sci.* **1**, 653–656.

McFadden L., McDonald E. V., Wells S., Anderson K., Quade J. and Forma S. L. (1998) The vesicular layer and carbonate collars of desert soils and pavements: age and relation to climate change. *Geomorphology* **24**, 101–145.

McKay D. S., et al. (1996) Search for past life on Mars: possible relic biogenic activity in Martian Meteorite ALH84001. *Science* **273**, 924–929.

Mickler P. J., Stern L. A. and Banner J. (2006) Large kinetic isotope effects in modern speleothems. *Geol. Soc. Am. Bull.* **118**, 65–81.

Nadelhoffer K. J. and Fry B. (1988) Controls on natural nitrogen-15 and carbon-13 abundances in forest soil organic matter. *Soil Sci. Soc. Am. J.* **52**, 1633–1640.

Nordt L. C., Hallmark C. T., Wilding L. P. and Boutton T. W. (1998) Quantifying pedogenic carbonate accumulations using stable carbon isotopes. *Geoderma* **82**, 115–136.

Quade J., Cerling T. E. and Bowman J. R. (1989) Systematic variation in the carbon and oxygen isotopic composition of Holocene soil carbonate along elevation transects in the southern Great Basin, USA. *Geol. Soc. Am. Bull.* **101**, 464–475.

Quade J., Cater J. M. L., Ojha T. P., Adam J. and Harrison T. M. (1995) Dramatic carbon and oxygen isotopic shift in paleosols from Nepal and late Miocene environmental change across the northern Indian sub-continent. *Geol. Soc. Am. Bull.* **107**, 1381–1397.

Rech J., Quade J. and Hart W. S. (2003) Isotopic evidence for the source of Ca and S in soil gypsum, anhydrite, and calcite in the Atacama Desert. *Geochim. Cosmochim. Acta* **67**, 575–586.

Richter J. (1987) *The Soil as a Reactor*. Catena Verlag, Cremlingen.

Romanek C. S., Grossman E. T. and Morse J. W. (1992) Carbon isotopic fractionation in synthetic aragonite and calcite: effects of temperature and precipitation rate. *Geochim. Cosmochim. Acta* **56**, 419–430.

Rundel P. W. and Mahu M. (1976) Community structure and diversity in a coastal fog desert in Northern Chile. *Flora* **165**, 493–505.

Rundel P. W., Dillon M. O., Palma B., Mooney H. A., Gulmon S. L. and Ehleringer J. R. (1991) The phytogeography and ecology of the coastal Atacama and Peruvian Deserts. *Aliso* **13**, 1–49.

Rundel P. W., Dillon M. and Palma B. (1996) Flora y vegetación del Parque Nacional Pan de Azúcar en el desierto de Atacama. *Gayana Botanica* **53**, 295–316.

Ruthsatz B. (1977) Pflanzengesellschaften und ihre Lebensbedingungen in den Andinen Halbwusten Nord-west-Argentiniens: Gottingen. *Dissertaciones Botanicae* **39**, 168.

Schenk H. J. and Jackson R. B. (2002) The global biogeography of roots. *Ecol. Monogr.* **72**(3), 311–328.

Searle A. and Rankin S. (1993) A preliminary petrographic study of the Chilean nitrates. *Geol. Mag.* **130**(30), 319–333.

Soloman D. K. and Cerling T. E. (1987) The annual carbon cycle in a montane soil; observations, modeling, and implications for weathering. *Water Resources Res.* **23**(12), 2257–2265.

Trewartha G. T. (1981) *The Earth's Problem Climates*. University of Wisconsin Press, Madison, Wisconsin, USA.

Trumbore S. E. (2000) Age of soil organic matter and soil respiration: radiocarbon constraints on belowground C dynamics. *Ecol. Appl.* **10**, 399–411.

Veit H. (1993) Upper Quaternary landscape and climate evolution in the norte Chico (northern Chile): an overview. *Mountain Res. Dev.* **13**, 139–144.

Villagrán C., Armesto J. J. and Kalin-Arroyo M. T. (1981) Vegetation in a high Andean transect between Turi and Cerro Leon in northern Chile. *Vegetatio* **48**, 3–16.

Villagrán C., Kalin-Arroyo M. T. and Marticorena C. (1983) Efectos de al desertizacion en al distribución de la flora andina de Chile. *Revista Chilena de Historia Natural* **56**, 137–157.

Vuille M. (1999) Atmospheric circulation over the Bolivian Altiplano during dry and wet periods and extreme phases of the Southern Oscillation. *Int. J. Climatol.* **19**, 1579–1600.

Ward D., Olsvig-Whittaker L. and Lawes M. (1993) Vegetation-environment relationships in a Negev Desert erosion cirque. *J. Veg. Sci.* **4**, 83–94.

Wedin D. A., Tieszen L. L., Dewey B. and Pastor J. (1995) Carbon isotope dynamics during grass decomposition and soil organic matter formation. *Ecology* **76**, 1383–1392.

Zhisheng A., et al. (2005) Multiple expansions of C_4 biomass in East Asia since 7 Ma coupled with strengthened monsoon circulation. *Geology* **33**(9), 705–708.

Associate editor: Stephan M. Kraemer